

ZENITH PASS PROBLEM IN AIR-TO-AIR MISSILES WITH NOD-OVER-  
ROLL GIMBAL

A THESIS SUBMITTED TO  
THE GRADUATE SCHOOL OF NATURAL AND APPLIED SCIENCES  
OF  
MIDDLE EAST TECHNICAL UNIVERSITY

BY

KUTLU DEMİR KANDEMİR

IN PARTIAL FULFILLMENT OF THE REQUIREMENTS  
FOR  
THE DEGREE OF DOCTOR OF PHILOSOPHY  
IN  
MECHANICAL ENGINEERING

JANUARY 2023



Approval of the thesis:

**ZENITH PASS PROBLEM IN AIR-TO-AIR MISSILES WITH NOD-OVER-ROLL GIMBAL**

submitted by **KUTLU DEMİR KANDEMİR** in partial fulfillment of the requirements for the degree of **Doctor of Philosophy in Mechanical Engineering, Middle East Technical University** by,

Prof. Dr. Halil Kalıpçılar  
Dean, Graduate School of **Natural and Applied Sciences** \_\_\_\_\_

Prof. Dr. M.A. Sahir Arıkan  
Head of the Department, **Mechanical Engineering** \_\_\_\_\_

Prof. Dr. Yiğit Yazıcıoğlu  
Supervisor, **Mechanical Engineering, METU** \_\_\_\_\_

**Examining Committee Members:**

Prof. Dr. Erhan İlhan Konukseven  
Mechanical Eng, METU \_\_\_\_\_

Prof. Dr. Yiğit Yazıcıoğlu  
Mechanical Eng, METU \_\_\_\_\_

Assoc. Prof. Dr. Ali Emre Turgut  
Mechanical Eng, METU \_\_\_\_\_

Assist. Prof. Dr. Kutluk Bilge Arıkan  
Mechanical Eng, TED University \_\_\_\_\_

Assist. Prof. Dr. Emir Kutluay  
Mechanical Eng, Hacettepe University \_\_\_\_\_

Date: 24.01.2023

**I hereby declare that all information in this document has been obtained and presented in accordance with academic rules and ethical conduct. I also declare that, as required by these rules and conduct, I have fully cited and referenced all material and results that are not original to this work.**

Name Last name : Kutlu Demir Kandemir

Signature :

## **ABSTRACT**

### **ZENITH PASS PROBLEM IN AIR-TO-AIR MISSILES WITH NOD-OVER-ROLL GIMBAL**

Kandemir, Kutlu Demir  
Doctor of Philosophy, Mechanical Engineering  
Supervisor : Prof. Dr. Yiğit Yazıcıoğlu

January 2023, 91 pages

Nod-over-Roll is a commonly used gimbal configuration in automatic target tracking and pointing systems due to its simplicity and volumetric advantage. Yet, it suffers from an inherent kinematic singularity problem right at the center of its task space, where roll axis and pointing vectors coincide. This phenomenon is called zenith pass problem and has to be solved in real time for a proper tracking performance. This thesis focuses on the zenith pass problem from an air-to-air missile seeker perspective. An estimator-based novel algorithm and a simulation environment has been developed. The performance of the proposed algorithm has been verified by a series of engagement scenario tests performed in comparison with available zenith-pass algorithms in the literature.

Keywords: Singularity, Air-to-Air Engagement, Zenith Pass Problem, Seeker, Gimbal

## ÖZ

### YUVARLANMA-YANDÖNME YERLEŞİMLİ HAVADAN HAVAYA FÜZE ARAYICILARINDA KUTUP GEÇİŞİ SORUNUNUN İNCELENMESİ

Kandemir, Kutlu Demir  
Doktora, Makina Mühendisliği  
Tez Yöneticisi: Prof. Dr. Yiğit Yazıcıoğlu

Ocak 2023, 91 sayfa

Yuvarlanma-yandönme yerleşimi; otomatik hedef takip ve işaretleme sistemlerine, hacimsel avantajı ve sadeliği sebebiyle tercih edilen bir kardan yapısıdır. Ancak görev uzayının tam ortasında, yuvarlanma ve yandönme eksenlerinin kesiştiği noktada kinematik tekillik bulunmaktadır ve bu nokta yakınlarındaki hareketleri kutup geçiş problemine maruz kalmaktadır. Hedef takip sisteminin işlevini yerine getirebilmesi için, kutup geçiş probleminin gerçek zamanlı olarak çözülmesi gerekmektedir. Bu tez, kutup geçiş problemini bir havadan havaya arayıcı başlık tasarımı bakış açısıyla ele almaktadır. Kestirimci tabanlı, yenilikçi bir kutup geçiş kontrol algoritması ve benzetim ortamı geliştirilmiştir. Önerilen algoritmanın başarımı, literatürdeki hazır algoritmalarla kıyaslamalı olarak gerçekleştirilen bir dizi eşleşme senaryosu testiyle doğrulanmıştır.

Anahtar Kelimeler: Tekillik, Hava-Hava Angajmanı, Kutup Geçiş Problemi, Arayıcı, Kardan

## ACKNOWLEDGMENTS

I wish to express my deepest gratitude to my supervisor Prof. Dr. Yiğit Yazıcıoğlu for his guidance, advice, criticism, encouragements and insight throughout the research.

I would like to express my sincere gratitude Prof. İlhan Konukseven and Assoc. Prof. Dr. Bülent İrfanoğlu for their suggestions and comments during my study.

I would would like to express my sincere gratitude to my former employer TÜBİTAK-SAGE and current employer ASELSAN A.Ş. for providing the necessary technical infrastructure and resources for the research conducted in this thesis. Their contribution was invaluable and greatly appreciated. I thank both companies for their support and for providing the necessary ecosystem during the research process.

I am deeply grateful to my mother Nimet who has been a constant source of love and support throughout my life. She has always believed in me, encouraged me and been there for me in this journey. I am also eternally grateful to my brother Kağan for his unwavering support and encouragement.

And lastly, to my beloved wife Çağıl, I cannot express enough gratitude for the love and support you have given me throughout my PhD journey. You have been my rock, my confidant, and my best friend. Thank you for making my life complete. I love you more than words can say. This thesis is dedicated to you, and our brilliant kids Mert Demir and Ada Bahar

## TABLE OF CONTENTS

ABSTRACT .....	v
ÖZ.....	vi
ACKNOWLEDGMENTS.....	vii
TABLE OF CONTENTS .....	viii
LIST OF TABLES .....	x
LIST OF FIGURES .....	xi
LIST OF ABBREVIATIONS .....	xiii
CHAPTERS	
1. INTRODUCTION.....	1
1.1. Motivation .....	1
1.2. Objectives and Scope .....	6
1.3. Dissertation Outlook.....	8
2. GIMBAL KINEMATICS AND ZENITH PASS PROBLEM .....	9
2.1. Zenith Pass Problem.....	9
2.2. Mathematical Formulation and Engagement Loop Analysis .....	10
2.2.1. Coordinate Frames and Transformations .....	11
2.2.2. Angular Position Analysis.....	13
2.2.3. Angular Rate Analysis.....	16
2.3. Mapping the Problem into a Unit Sphere .....	18
2.3.1. Angular Position Analysis.....	20
2.3.2. Angular Velocity Analysis .....	23
2.4. Results of Engagement Loop Analysis.....	24
2.5. Critical ATTPS components affecting tracking performance .....	25
2.5.1. Field of View and Field of Regard.....	25
2.5.2. Target Manoeuvrability .....	27
2.5.3. Gimbal Rate Limit and Controller.....	27
2.5.4. Tracker.....	28



3. SYSTEM MODEL AND ENGAGEMENT SCENARIOS .....	31
3.1. Simulation Model.....	31
3.1.1. Gimbal and Control System Model .....	35
3.1.2. Target Tracker Model .....	39
3.1.3. Zenith Pass Algorithm .....	44
3.2. Exemplary Scenarios .....	46
3.2.1. Scenario 1.....	48
3.2.2. Scenario 2.....	50
3.2.3. Scenario 3.....	52
3.2.4. Scenario 4.....	54
3.2.5. Scenario 5.....	56
4. ZENITH PASS ALGORITHMS .....	59
4.1. Zenith Pass Algorithm Solutions In Literature .....	59
4.2. Baseline Algorithms.....	61
4.2.1. ZPA0 .....	62
4.2.2. ZPA1 .....	63
4.3. Proposed Zenith Pass Algorithm (ZPA2) .....	64
5. TESTS AND VERIFICATION .....	71
5.1. Performance criterion.....	71
5.2. Test Matrix.....	71
5.3. Test Results.....	72
6. RESULTS AND DISCUSSION .....	77
6.1. Performance of Zenith Pass Algorithms .....	77
6.2. Discussion .....	84
6.3. Further Study .....	85
REFERENCES .....	87
CURRICULUM VITAE.....	91

## LIST OF TABLES

### TABLES

Table 5.1. Test Configurations .....	72
Table 5.2. Test Results .....	72
Table 6.1. Scenario 1 results (ZPA0 vs ZPA2) .....	78
Table 6.2. Scenario 2 results (ZPA0 vs ZPA2) .....	79
Table 6.3. Scenario 3 results (ZPA1 vs ZPA2) .....	80

## LIST OF FIGURES

### FIGURES

Figure 1.1. A Pedestal 2-Axis High Accuracy Stabilized Gimbal (HASG) for Aerial Target Tracking.....	4
Figure 1.2. Gimbal tilting method to avoid singularity[6].....	5
Figure 1.3. Nod-over-roll gimbal, kinematic representation .....	6
Figure 2.1. Engagement Vector Loop and Coordinate Frames.....	11
Figure 2.2. Field of View and Field of Regard .....	26
Figure 2.3. ATTPS Control Topology .....	28
Figure 3.1. System Block Diagram.....	32
Figure 3.2. Simulation Overview .....	34
Figure 3.3. Roll and Nod Gimbal Models.....	36
Figure 3.4. 2-Axis Gimbal Control Model.....	37
Figure 3.5. Rate Loop Controller Design.....	38
Figure 3.6. Closed Loop Bode Diagrams of Some of the Tuned Rate Controllers	39
Figure 3.7. Tracker Block Diagram – Top Level.....	40
Figure 3.8. Rate Tracker – Middle Level.....	42
Figure 3.9. Rate Tracker – Bottom Level .....	43
Figure 3.10. ZPA – Top Level .....	45
Figure 3.11. ZPA Bottom Level: ZPA0 Kinematic Inversion .....	46
Figure 3.12. Scenario 1 – Path 3D View .....	49
Figure 3.13. Scenario 1 - Trajectories.....	50
Figure 3.14. Scenario 2 – Path 3D View .....	51
Figure 3.15. Scenario 2 - Trajectories.....	52
Figure 3.16. Scenario 3 – Path 3D View .....	53
Figure 3.17. Scenario 3 - Trajectories.....	54
Figure 3.18. Scenario 4 – Path 3D View .....	55
Figure 3.19. Scenario 4 - Trajectories.....	56
Figure 3.20. Scenario 5 – Path 3D View .....	57

Figure 3.21. Scenario 5 - Trajectories .....	58
Figure 4.1. ZPA0 Block Diagram.....	62
Figure 4.2. ZPA1 Block Diagram.....	64
Figure 4.3. ZPA2 Kalman Filter Predictions – Schematic Diagram .....	65
Figure 4.4. ZPA2 Block Diagram.....	67
Figure 4.5. ZPA2 implementation in Stateflow.....	70
Figure 6.1. Results of an exemplary scenario run -Trajectory (ZPA2, Scenario 2)	77
Figure 6.2. Results of an exemplary scenario run -Test Data (ZPA2, Scenario 2)	78
Figure 6.3. ZPA2 performance under Scenario 4. Trajectory .....	82
Figure 6.4 ZPA2 performance under Scenario 4. Test Data .....	82
Figure 6.5. ZPA2 performance under Scenario 5. Trajectory .....	83
Figure 6.6. ZPA2 performance under Scenario 5. Test data .....	84

## LIST OF ABBREVIATIONS

### ABBREVIATIONS

ATTPS	Automatic Target Tracking and Pointing System
ZPA	Zenith Pass Algorithm
ZPA0/1/2	Specific ZPAs developed in this study
ZP	Zenith Pass
LOS	Line of Sight
R.H.S.	Right-Hand Side
L.H.S.	Left-Hand Side
W.R.T.	with respect to



# CHAPTER 1

## INTRODUCTION

This chapter presents a brief introduction to the zenith pass problem and provides a basic understanding on how the problem is handled in this study. After summarizing the objectives and scope, the outlook of the dissertation is briefly summarized in the last part.

### 1.1. Motivation

Automatic target tracking and pointing systems (ATTPS) point or track targets in 3D space employing a multi-axis gimballed mechanism. It has a wide field of use, from missile seekers to satellite trackers or webcam suites.

As discussed in the following sections, ATTPS involve various mechanic, electronic and algorithmic sub-systems. Therefore, ATTPS design can lead to a relatively complex optimization problem depending on the system requirements. Like most system designs, minimizing SWaP-C (size-weight-power-cost) is the driving force while platform requirements affect its construction significantly.

ATTPS design is an interdisciplinary work including kinematics, mechanics, control theory, optics, signal and image processing. Various system parameters (track rate, gimbal axis configuration, pixel size, field of view, field of regard etc.) are interlinked to some extent and directly influence system performance. This intricate nature necessitates a systematic design approach, using different engineering disciplines, concerning the system requirements.

A typical 2-axis ATTPS components can be explained hierarchically as follows:

- 1) Gimballed Pointing System

- a) Imaging System: The gimbal's main payload comprises optical components to construct an image on the detector to be used in target tracking.
  - b) Electromechanical Structure: Servomotors, resolvers, encoders and mechanics that build up the 2-axis gimbal mechanism.
  - c) Gimbal Control Software: A servo control algorithm working on gimbal axes to realize commands received from target tracking system
- 2) Target Tracking System
- a) Image Tracker Algorithm: Software for discriminating and tracking the target in a dynamic cluttered scene using the optical and kinetic data observed from the Gimballed Pointing System. Many different image tracking algorithms exist, like pattern matching, feature tracking, and object recognition. A summary of those algorithms are given in [1]
  - b) Gimbal Command Generator: Software for generating real-time commands for the gimbal for tracking and the platform for guidance. Those commands shall be tailored for engagement condition and gimbal kinematics. This part is where the zenith pass algorithm is implemented.

Given that generic structure, a 2-axis gimbal has variety of uses in engineering field

In missile guidance problem, it is vital to observe the states of the target during the flight up to intercept. This type of guidance is referred as homing guidance, which is widely used in air-to-air, air-to-ground, and surface-to-air missiles. The concept requires the missile to sense the target by some means and guide itself to the target by sending commands to its control surfaces [2]. Sensing, observing and command generating tasks are handled by the seeker subsystem, which is an elegant example of APPTS.

In air-to-air missiles, the most widely used gimbal configuration includes two orthogonal axes, which is mechanically simple and covers a relatively large FOR. Depending on the application requirements, orientation of the axes may change.

Conceptually, there are two gimbal arrangements as nod-over-roll and yaw-pitch. Nod-over-roll configurations tend to consume less volume due to small packing and



are preferred for high off-boresight scenarios because small inertia means fast response. However, for targets at the center of the FOR a kinematic singularity exists causing divergent gimbal rate commands. This problem requires a specialized gimbal steering algorithm for this region. In contrast, yaw-pitch gimbals are larger, have higher inertia and hence a slower response time however, they do not magnify the sight-line rate error anywhere within the FOR. [3]

Nod-over roll configuration is superior in terms of FOR and track rate. The roll axis coincides with the missile body axis and has full turn capability with the help of a slip ring. Yet, it requires a more complicated design. Although being slower and having a smaller off-boresight angle, a pitch-yaw configured gimbal comes forward with its simplicity.

Consider a missile seeker gimbal with 1-3 sequence (a.k.a. nod-over roll). Despite being a desired engagement condition from flight mechanics perspective, when the missile is headed directly towards the target, there is a risk of having LOS vector aligned with roll axis of the gimbal. As stated earlier in literature survey, the condition is called as zenith pass or nadir.

In the vicinity of nadir, commanding the gimbal to keep tracking the target with zero boresight error yields impulsive velocity commands for roll axis which are beyond the capability of its servomechanism. As a result, significant tracking error accumulates as well motion blur occur in the captured image sequence. When the tracking error exceeds FOV cone, or the image tracker algorithm cannot discriminate the target in the blurred image then the lock-on is lost and mission fails. This region inside which conventional tracking is not possible is called as the 'nadir cone' [4] or 'cone of occlusion'[5].

The same problem is also valid for pedestal aerial target tracking systems. The primary difference from previous case is having a fixed base rather than a moving one in problem formulation.

For both missile seekers and pedestal ATTPS the free variable is target motion. In other words, system has no control over the target trajectory, therefore although being a low probability, zenith pass might occur during mission and it has to be handled carefully. Those two types of systems can be regarded as free target trackers.

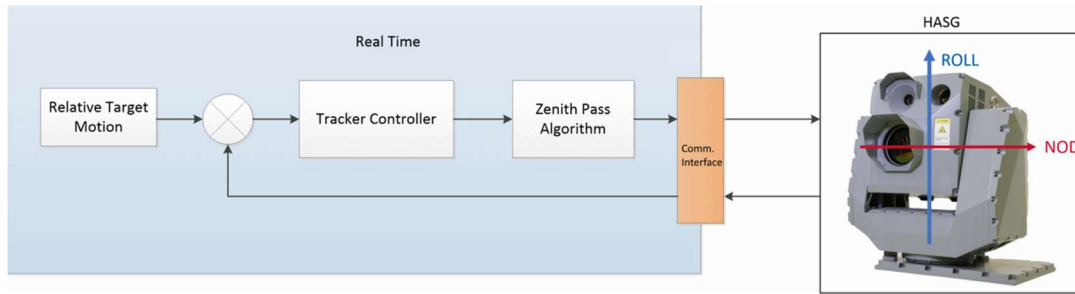


Figure 1.1. A Pedestal 2-Axis High Accuracy Stabilized Gimbal (HASG) for Aerial Target Tracking

Another type of ATTPS is ground based celestial trackers which are designed to track satellites or astronomical bodies having known trajectories. Such systems are much bigger in size, and the angular rate of the gimbal is mostly determined by earth's rotation speed, which is quite small compared to that of a missile seeker or pedestal tracker.

Although being a completely different problem, when the unit under track passes from the top, it reduces to the same singularity problem kinematically. However, the antenna has much slower angular rates when compared to a missile seeker.

When the tracked item (whether a satellite or an astronomical object) passes close to the zenith, the rate demands rise up and there is a risk of chatter or saturating the servo.

In such systems, one common approach is to tilt the base of the mechanism in a controlled way to avoid near-zenith pass conditions [6]. This method can be regarded as adding a temporary third gimbal axis to the system.

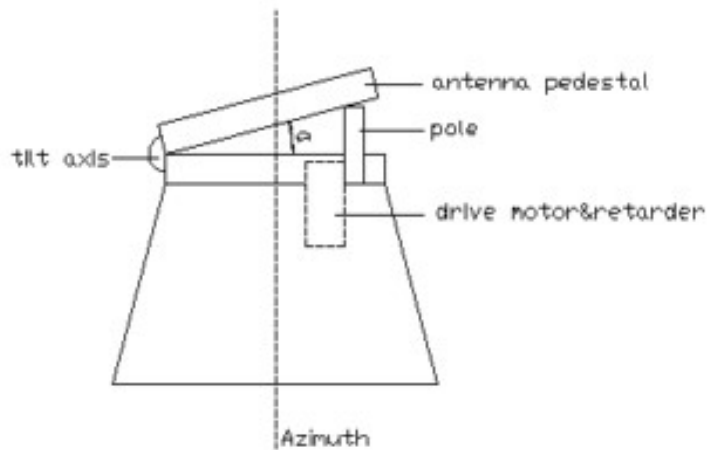


Figure 1.2. Gimbal tilting method to avoid singularity[6]

Another way to attack the problem in such tracking antennas is utilizing the apriori target trajectory. The antenna servos are moved faster than the target near the singularity zone preemptively, to meet with the tracked object at the exit. The track is intentionally degraded for a short duration, on the other hand any risk of saturation or chatter is eliminated. [7]

The most significant difference between celestial trackers and free target trackers is that, the target trajectory is predetermined, which enables the user to calculate pointing error and try to minimize it analytically. However, this is definitely not the case for the latter.

An ATTPS design starts with selecting the number of gimbal axes to be implemented. For the sake of simplicity, size and cost it is very desirable to keep the gimbal degree-of-freedom at 2, which is the minimum. Yet, this selection brings the pitfall of zenith pass (ZP) problem, which may yield complete loss of function at some specific gimbal orientations. Therefore, the design boils down to a tradeoff between system complexity and performance degradation.

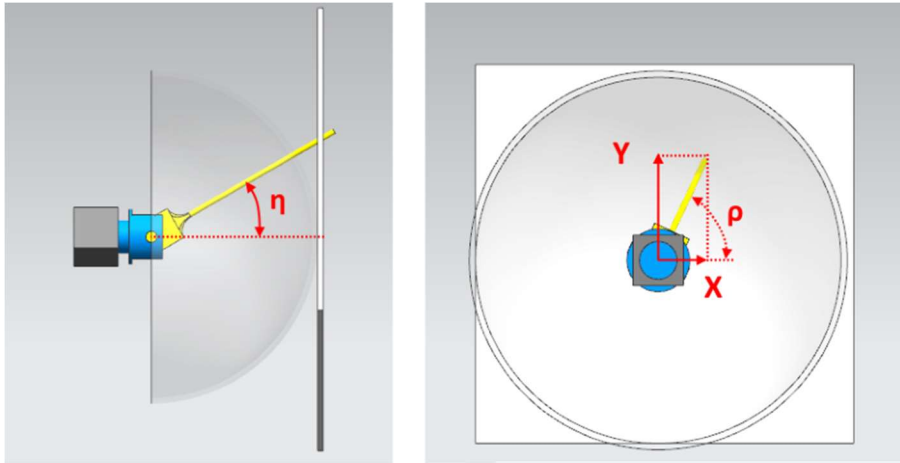


Figure 1.3. Nod-over-roll gimbal, kinematic representation

Engineers have tried various methods to cover up the void created by singular gimbal configurations in 2-axis gimbals. Proposed solutions mostly remain specific to the application field because of the lack of a generalized approach.

The motivation behind this work is to evaluate the zenith pass problem with a generalized approach to cover all aspects of free target tracking APPTS, analyze the literature and contribute to this field by a new zenith pass algorithm (ZPA) solution.

## 1.2. Objectives and Scope

From robot kinematics perspective, 2-axis gimbal is a spherical serial manipulator with two orthogonal axes, capable of scanning a hemisphere. Target is moving on this spherical surface and gimbal is expected to point it with regard to the angle and rate commands generated by the tracker. If not handled properly, direct kinematic inversion can cause infinitely large rate commands when the target is in the vicinity of zenith zone.

Mathematically, ZP problem of a 2-axis gimbal can be expressed as; investigating the singular configurations of a non-redundant R2 robotic system. It is vital to note that, although a rigorous mathematical foundation is provided, this work is not aiming to provide a generalized singularity analysis of robotic systems. As seen in

the related chapters, after a structured mathematical formulation is presented, the focus will shift to 2-DOF gimbals having singularity point within their task space. In addition, the nature of target tracking requires real time solution of Inverse Kinematics Problem (IKP) of the gimbal. This also brings a multiple solution problem which has to be handled properly.

As a result of this complicated nature, one critical step to move forward is to build up a test bench involving all necessary system parameters, on which the ZPA's will be verified. This setup shall reflect the gimbal, gimbal control algorithm, target, tracker and ZPA behavior correctly.

Based on the summarized definitions and assumptions, the objectives of this thesis are declared as follows:

- Provide a mathematical background on gimbal kinematics and singularity
- Create a detailed ATTPS simulation environment involving
  - Means to implement target dynamics and sensor characteristics
  - A detailed 2-axis gimbal model and gimbal servo controllers
  - Means to implement different zenith pass algorithms
  - Means to investigate the effect of specific parameters on ATTPS performance near zenith
- Propose a novel zenith pass algorithm and compare them with available solutions in literature by making use of this simulation environment.

Although the singularity problem is discussed in general terms, simulations and formulations have been developed for the air-to-air missile option, as it gives the most challenging dynamical conditions. Even the dissertation title implies that the work is on air-to-air missile seekers, it can be generalized to any kind of nod-over-roll configured ATTPS.

### 1.3. Dissertation Outlook

The dissertation is organized under 6 Chapters

Chapter 2 examines the Zenith Pass Problem by starting from its formal definition. A detailed mathematical formulation of engagement is presented which is followed by a simplified version of the same analysis, to be used in the forthcoming simulation chapters.

Chapter 3 presents the details of generated simulation environment for studying ZPA. The critical sub-systems having a physical correspondence on ATTPS are dissected and explained in detail. The critical design choices and assumptions affecting ATTPS behavior are presented. Out of three zenith pass algorithms proposed; first two (ZPA0 and ZPA1) corresponds to standard solutions, that are prone to track loss around zenith, and the last one, ZPA2, is the novel solution developed in this study. In the closure of the chapter, exemplary test scenarios to be used for benchmarking ZPA's are given.

Chapter 4 extends the analysis in previous section and zooms in the ZPA2 algorithm developed. The design choices, novelty, implementation details of the developed algorithm are expressed.

Chapter 5 provides the test results obtained from simulations conducted with aforementioned test scenarios in Chp3. By the help of simulation runs, performance of ZPA2 is numerically evaluated compared to baseline solutions.

Chapter 6 summarizes the results of this study, evaluates the contribution to the literature and outlines further research directions on this field.

## CHAPTER 2

### GIMBAL KINEMATICS AND ZENITH PASS PROBLEM

This section provides a foundation for the following chapters. Starting with general definitions on singularity in roll-over-nod configured ATTPS, zenith pass problem, notation conventions and loop closure equation of engagement, gimbal dynamics will be formulated. Zenith condition will show up as a byproduct in terms of specific initial conditions in the differential equations.

Each and every critical sub-component of an ATTPS is modeled in a simulation environment. Several critical parameters are varied through the analysis and their effect on ZP performance is sought.

#### 2.1. Zenith Pass Problem

As explained in Chapter 1, this work specifically focuses on free target tracking ATTPS employing a nod-over-roll gimbal and therefore following analysis is valid for that.

The roll-over-nod gimbal is a 2-axis non-redundant serial manipulator. When roll axis coincides with line-of-sight vector, the phenomenon called zenith pass occurs. At that instant, Jacobian is not invertible and inverse instantaneous kinematics becomes indeterminate. Therefore, from a mathematical perspective, zenith pass problem can be classified as an inverse instantaneous kinematics problem (IIKP) [8].

Kinematic singularities in serial manipulators have been studied extensively in the field of Robotics. Most of the notable work approach the singularity problem by showing the rank deficiency in Jacobian matrix [9] [10] [11]. Extracting the singular configurations by analytic, numeric and geometrical methods and finding ways to

avoid those specific kinematic conditions is generally preferred in literature, yet such work addresses mainly inverse kinematics problem of industrial robotic arms having degrees of freedom larger than 2.

In addition to the singularity at nadir, the roll-nod seeker has an intrinsic double solution property in the whole task space, which has to be handled separately.

## 2.2. Mathematical Formulation and Engagement Loop Analysis

The preliminaries on coordinate frame transformations, vector algebra is given in the APPENDIX. Reader is directed to that section to be able to follow the formulation presented herein. The formulation presented below is published in [12]

To give a better understanding, inverse kinematic solution will be sought by solving for loop closure equation. For the sake of generality, a missile-target engagement scenario is taken into account where the target and the base frame of ATTPS (missile) is allowed to move. Before start, the important assumptions are listed as follows:

1. The gimbal is in nod-over-roll configuration with a hemispherical coverage. The nod angle is allowed to move between  $[-\frac{\pi}{2}, \frac{\pi}{2}]$  and the nod angle of zero corresponds to zenith. The roll angle is full turn capable  $[0, 2\pi]$ .
2. The missile and the target are moving freely in the 3D cartesian space, and at a specific instant, the seeker points to the target
3. The missile, the target and the seeker are assumed to be fully observable.

Those might seem counterintuitive for a realistic pursuing scenario. However, the aim is to derive the formulation with respect to engagement parameters, therefore the reader is kindly requested to accept the assumptions as true for now.



The formulation begins with the engagement loop of this configuration, which is illustrated in below figure.

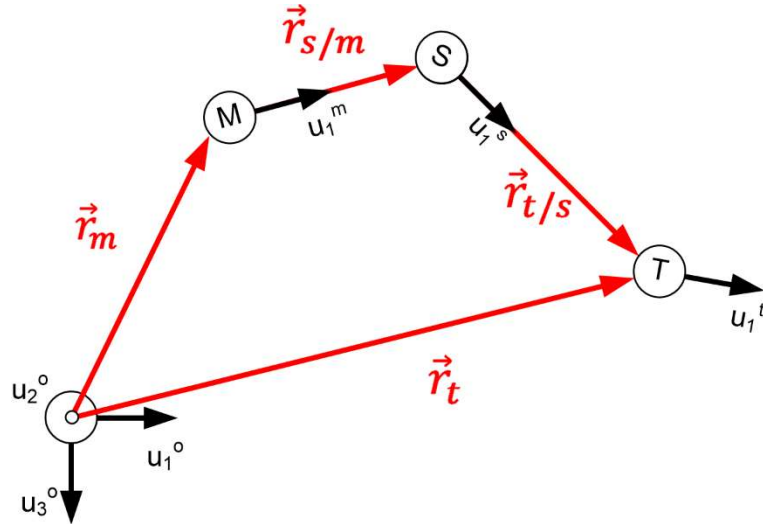


Figure 2.1. Engagement Vector Loop and Coordinate Frames

### 2.2.1. Coordinate Frames and Transformations

The following coordinate frames are defined in North-East-Down (NED) convention

- Inertial Coordinate Frame ( $\mathcal{F}_o$ ) : Fixed to the ground. Geographic effects neglected.
- Platform Coordinate Frame ( $\mathcal{F}_m$ ) : Attached to the missile center-of-gravity (CoG). The rotational transformation between inertial CF to the missile CF is defined in 3-2-1 Euler rotation sequence as follows:

$$\begin{array}{ccccccc} & \vec{u}_3^{(o)} & \vec{u}_2^{(a)} & \vec{u}_1^{(b)} & & & \\ \mathcal{F}_o & \rightarrow & \mathcal{F}_a & \rightarrow & \mathcal{F}_b & \rightarrow & \mathcal{F}_m \\ & \psi & \theta & \phi & & & \end{array} \quad (1)$$

Where a, and b denotes the intermediate CFs of 3-2-1 rotation sequence.  $\psi$ ,  $\theta$  and  $\phi$  correspond to the successive yaw, pitch and roll angles of the missile. The resultant transformation matrix for the above sequence is:

$$C^{(0,m)} = C^{(0,a)}C^{(a,b)}C^{(b,m)} \quad (2)$$

$$C^{(0,m)} = \begin{bmatrix} c\psi & -s\psi & 0 \\ s\psi & c\psi & 0 \\ 0 & 0 & 1 \end{bmatrix} \times \begin{bmatrix} c\theta & 0 & s\theta \\ 0 & 1 & 0 \\ -s\theta & 0 & c\theta \end{bmatrix} \times \begin{bmatrix} 1 & 0 & 0 \\ 0 & c\phi & -s\phi \\ 0 & s\phi & c\phi \end{bmatrix} \quad (3)$$

$$C^{(0,m)} = \begin{bmatrix} c\psi c\theta & (c\psi s\phi s\theta - s\psi c\phi) & (s\psi s\phi + c\psi c\phi s\theta) \\ s\psi c\theta & (c\psi c\phi - s\psi s\theta s\phi) & (s\psi s\theta c\phi - c\psi s\phi) \\ -s\theta & s\phi c\theta & c\phi c\theta \end{bmatrix} \quad (4)$$

Target Coordinate Frame ( $\mathcal{F}_t$ ) : Fixed to the target CoG. Here, the target is modeled as a moving point mass in 3-D space, therefore its angular orientation has no functional significance.

Seeker LOS Coordinate Frame ( $\mathcal{F}_s$ ) : Fixed to the Seeker's true Line of Sight (LOS).  $\rho$  and  $\eta$  correspond to the roll and nod angles of the gimbal. The rotational transformation between missile and seeker LOS CFs is:

$$\begin{array}{ccccccc} & \vec{u}_1^{(m)} & \vec{u}_3^{(e)} & & & & \\ \mathcal{F}_m & \rightarrow & \mathcal{F}_e & \rightarrow & \mathcal{F}_s & & \\ & \rho & \eta & & & & \end{array} \quad (5)$$

Where subscript e denotes the CF fixed to the roll axis. The corresponding transformation matrix for the above sequence is:

$$\mathcal{C}^{(m,s)} = \mathcal{C}^{(m,e)} \mathcal{C}^{(e,s)} \quad (6)$$

$$\mathcal{C}^{(m,s)} = \begin{bmatrix} 1 & 0 & 0 \\ 0 & c\rho & -s\rho \\ 0 & s\rho & c\rho \end{bmatrix} \times \begin{bmatrix} c\eta & -s\eta & 0 \\ s\eta & c\eta & 0 \\ 0 & 0 & 1 \end{bmatrix} \quad (7)$$

$$\mathcal{C}^{(m,s)} = \begin{bmatrix} c\eta & 0 & s\eta \\ s\eta & s\rho & c\rho & -c\eta & s\rho \\ -c\rho & s\eta & s\rho & c\eta & c\rho \end{bmatrix} \quad (8)$$

### 2.2.2. Angular Position Analysis

Given above coordinate frames, now it is possible to study the *inverse kinematics problem* aiming to find the joint variables corresponding to a given end-effector position and orientation. The solution to angular position analysis has a great importance in order to transform the motion specifications, assigned to the end-effector in the operational space, into the corresponding joint space motions. The analysis may yield multiple solutions, or even infinitely many solutions. [13]

The vector loop illustrated in Figure 2.1 is expressed as:

$$\vec{r}_{t/s} = \vec{r}_t - \vec{r}_m - \vec{r}_{s/m} \quad (9)$$

Note that the seeker is fixed to missile body, therefore  $\vec{r}_{s/m}$  is a constant vector in  $\mathcal{F}_m$ , along  $\vec{u}_1^{(m)}$ , where  $d$  is the axial distance between missile center-of-gravity and gimbal. Note that for the time being,  $d$  is assumed to be known.

$$\vec{r}_{s/m} = d\vec{u}_1^{(m)} \quad (10)$$

Resolving vectors in earth-fixed frame yields the following matrix equality.

$$\bar{r}_{t/s}^{(0)} = \bar{r}_t^{(0)} - \bar{r}_m^{(0)} - d\hat{C}^{(0,m)}\bar{u}_1^{(m)} \quad (11)$$

$$\bar{r}_{t/s}^{(0)} = \begin{bmatrix} x_t \\ y_t \\ z_t \end{bmatrix} - \begin{bmatrix} x_m \\ y_m \\ z_m \end{bmatrix} - d \begin{bmatrix} c\psi c\theta \\ s\psi c\theta \\ -s\theta \end{bmatrix} \quad (12)$$

$$\bar{r}_{t/s}^{(0)} = \begin{bmatrix} x_t - x_m - d(c\psi c\theta) \\ y_t - y_m - d(s\psi c\theta) \\ z_t - z_m + d s\theta \end{bmatrix} \quad (13)$$

Note that the right-side parameters in ( 13 ) are known, therefore  $\bar{r}_{t/s}^{(0)}$  can be calculated at every instant of the engagement analysis. The next step is to extract gimbal angles for successful pointing. The seeker pointing vector  $\vec{r}_{t/s}$  is along  $\bar{u}_1^{(s)}$ . The gimbal angles correspond to the Euler angles of the transformation from  $\mathcal{F}_m$  to  $\mathcal{F}_s$ . Expressing the pointing vector in seeker frame yields:

$$\vec{r}_{t/s} = |\vec{r}_{t/s}| \bar{u}_1^{(s)} \quad (14)$$

$$\bar{r}_{t/s}^{(m)} = |\vec{r}_{t/s}| \hat{C}^{(m,s)} \bar{u}_1^{(s)} \quad (15)$$

$$\bar{r}_{t/s}^{(m)} = |\vec{r}_{t/s}| \begin{bmatrix} c\eta \\ s\eta s\rho \\ -c\rho s\eta \end{bmatrix} \quad (16)$$

$\bar{r}_{t/s}^{(m)}$  can be expressed in Inertial reference frame by:

$$\bar{r}_{t/s}^{(m)} = \hat{C}^{(m,0)} \bar{r}_{t/s}^{(0)} \quad (17)$$

Where  $\hat{C}^{(m,0)}$  is the transpose of ( 4 ). Inserting ( 17 ) into ( 16 ):

$$\hat{C}^{(m,0)} \bar{r}_{t/s}^{(0)} = |\vec{r}_{t/s}| \begin{bmatrix} c\eta \\ s\eta \ s\rho \\ -c\rho \ s\eta \end{bmatrix} \quad (18)$$

$$\hat{C}^{(m,0)} \frac{\bar{r}_{t/s}^{(0)}}{|\vec{r}_{t/s}|} = \begin{bmatrix} c\eta \\ s\eta \ s\rho \\ -c\rho \ s\eta \end{bmatrix} \quad (19)$$

Note that  $|\vec{r}_{t/s}|$  is the length and can be calculated from ( 13 ). Left-hand side of ( 19 ) is all known and the result is symbolized with 3-element k vector as follows:

$$\hat{C}^{(m,0)} \frac{\bar{r}_{t/s}^{(0)}}{|\vec{r}_{t/s}|} = \begin{bmatrix} k_1 \\ k_2 \\ k_3 \end{bmatrix} = \begin{bmatrix} c\eta \\ s\rho \ s\eta \\ -c\rho \ s\eta \end{bmatrix} \quad (20)$$

From first row, nod angle ( $\eta$ ) can be calculated with one sign ambiguity:

$$\cos \eta = k_1 \rightarrow \sin \eta = \sigma \sqrt{1 - k_1^2}, \quad (\sigma = \pm 1) \quad (21)$$

$$\eta = \text{atan2} \left( \sigma \sqrt{1 - k_1^2}, k_1 \right) \quad (22)$$

Using second and third rows of ( 20 ) one may find the roll angle with the same sign ambiguity as follows:

$$\mathbf{if} \ \eta \neq \mathbf{0}, \quad \sin(\rho) = \frac{k_2}{\sin(\eta)} \quad (23)$$

$$\text{if } \boldsymbol{\eta} \neq \mathbf{0}, \quad \cos(\rho) = \frac{k_3}{-\sin(\eta)} \quad (24)$$

$$\rho = \text{atan2}(\sigma k_2, -k_3), \text{ if } \eta \neq 0, \quad (\sigma = \pm 1) \quad (25)$$

When the missile and the target positions and missile orientation are available for a specific instant, the corresponding gimbal angles can be calculated with the above formulation.

The first implication of the inverse kinematics problem solution is that, there is one sign ambiguity at ( 21 ), which manifests itself as a double valuedness in the entire task space.

Secondly, for roll angle equations ( 23 ) - ( 25 ) give valid solutions if and only if nod angle is not equal to zero. As the nod angle approaches towards zero, division by zero error will occur and roll angle will be indeterminate.

The angular position analysis showed that when the nod angle is zero, (i.e. the target is at zenith position) there is a kinematic singularity causing infinitely many solutions for the roll angle. Therefore, the analysis proves that the vicinity of zenith zone has to be handled carefully and separately for target tracking.

Secondly, there is an inherent sign ambiguity for roll-over-nod gimbal within the entire task space. For any non-singular orientation, there exists two distinct solutions for gimbal angles and it is necessary to develop an algorithm to select the proper one. One practical way of doing is monitoring previous roll angle and select the solution that requires the smallest roll movement.

### 2.2.3. Angular Rate Analysis

For predefined trajectories, seeker reference angular rates can also be extracted. Differentiating the vector loop equation ( 9 ) w.r.t. inertial CF yields the following velocity equation.

$$D_o(\vec{r}_{t/s}) = D_o(\vec{r}_t) - D_o(\vec{r}_m) - D_o(\vec{r}_{s/m}) \quad (26)$$

Using vector algebra, it is possible to expand ( 26 ) as follows:

$$D_s(\vec{r}_{t/s}) + \vec{\omega}_{s/o} \times \vec{r}_{t/s} = \vec{V}_t - \vec{V}_m - \vec{\omega}_{m/o} \times \vec{r}_{s/m} \quad (27)$$

$$(\vec{\omega}_{s/m} + \vec{\omega}_{m/o}) \times \vec{r}_{t/s} = \vec{V}_t - \vec{V}_m - \vec{\omega}_{m/o} \times d\vec{u}_1^m - D_s(\vec{r}_{t/s}) \quad (28)$$

$$\vec{\omega}_{s/m} \times \vec{r}_{t/s} = \vec{V}_t - \vec{V}_m - D_s(\vec{r}_{t/s}) - \vec{\omega}_{m/o} \times d\vec{u}_1^m - \vec{\omega}_{m/o} \times \vec{r}_{t/s} \quad (29)$$

Each parameter in ( 29 ) is known except  $\vec{\omega}_{s/m}$ , which implicitly contains roll and nod gimbal rates. The seeker is restricted to rotate along  $\vec{u}_1^{(o)}$  and  $\vec{u}_3^{(e)}$  axes. Utilizing the additive property of angular velocities in 3-d kinematics,  $\vec{\omega}_{s/m}$  can be expressed in terms of roll and nod rates (w.r.t. missile body) as follows:

$$\vec{\omega}_{s/m} = \rho_r \vec{u}_1^{(m)} + \eta_r \vec{u}_3^{(e)} \quad (30)$$

$$\vec{\omega}_{s/m}^{(m)} = \rho_r \vec{u}_1 + \eta_r \hat{C}^{(m,e)} \vec{u}_3 \quad (31)$$

Using ( 31 ) in ( 29 ) may yield the Jacobian matrix in the following form:

$$[\vec{V}_t - \vec{V}_m] = J \begin{bmatrix} \dot{\eta} \\ \dot{\rho} \\ \dot{\psi} \\ \dot{\theta} \\ \dot{\phi} \end{bmatrix} \quad (32)$$

Note that above formulation states that, in order to define end effector position, one shall set not only gimbal angles, but also missile orientation angles. This results in a Jacobian matrix of size  $3 \times 5$ .

However, since both missile and target kinematic parameters are involved, there are redundant terms in the Jacobian that yield a non-square matrix. The equations become way more complex and it is harder to make conclusions on roll and nod angles and their rates among them. For that reason, a simplified analysis is conducted in the following part.

### **2.3. Mapping the Problem into a Unit Sphere**

ZP is an angular motion problem around a specific zone, therefore it is worth to simplify the analysis with regard to gimbal angles. The inverse kinematic solution presented in the previous section approach the problem in a generalized manner and therefore mathematically complex. A simpler approach is necessary to focus on the gimbal singularity.

If the problem is mapped into a unit sphere, where the roll-nod seeker is located in the center with a constrained pointing vector in 1-3 Euler rotation sequence; and the target is constrained to move on the sphere surface with respect to 3-2 Euler rotation sequence, it would be much easier to generate exemplary engagement scenarios and study the singularity of the gimbal around nadir zone. In fact, when the gimbal controller and the tracker algorithms work together under an ATTPS scheme, such a mapping naturally exists. It is generally preferred to use a singularity free reference frame for the tracker (3-2 Euler rotation in this case) The gimbal reference frame is dictated by mechanical structure (1-3 Euler rotation) which is susceptible to both singularity and double solution. An algorithmic block exists in between target tracker outputs (3-2 sequence) and gimbal inputs (1-3 sequence) which also handles the zenith pass and double solution problems. A similar approach is given by [14]



Note that this approach is similar to fixing the missile seeker in previous analysis to a pedestal and projecting the target position to a unit circle around it.

This simplification would manifest itself by a single vector equality. The previous generalized approach utilize cartesian coordinates of the target and the platform to solve for gimbal angles, and it required a bold assumption as full state observability for all systems. In fact, from ATTPS point of view, everything happens inside a unit sphere, regardless of the translational distance between target and the platform. The relative distance rate to the target cannot be observed but ‘guesstimated’[2] by guidance and navigation computer. Therefore, the left-hand side parameters of ( 32 ) are simply unknowns for the gimbal unit itself.

It would be convenient to limit the problem to the front hemisphere by restricting target azimuth angle to  $-\pi < \psi_t < \pi$  and elevation angle to  $-\frac{\pi}{2} < \theta_t < \frac{\pi}{2}$ . This way, target CF will be singularity free and it will be possible to define any kind of target movement without mathematical complexity. The gimbal CF however will face the inevitable kinematic singularity and double valuedness problems, which are the focus of this thesis work.

This way it is possible to focus on angular displacements/rates and study the singularity without the computational load caused by platform or target’s translational motions.

The aim of this work is to build up a mapping block in between by considering zenith pass and double solution problems in real time. The overall problem reduces into 4 variables. Elevation and azimuth angle of the target defines target position and they constitute the inputs coming from the tracker in a singularity-free frame. Roll and nod rate commands are the outputs which are fed to the gimbal controller as commands.

By the help of above assumptions, a simplified kinematic analysis on unit sphere can be conducted. A similar scheme will be followed such that, IKP is solved for angular position analysis, and dynamic Jacobian is solved for angular rate analysis.

### 2.3.1. Angular Position Analysis

Angular position analysis on unit sphere starts with simplifying equation ( 5 ) yields the target CF orientation w.r.t. inertial CF in 3-2 Euler rotation sequence:

$$\begin{array}{ccc} \vec{u}_3^{(o)} & \vec{u}_2^{(c)} & \\ \mathcal{F}_o \rightarrow \mathcal{F}_c \rightarrow \mathcal{F}_t & & \\ \psi_t & \theta_t & \end{array} \quad (33)$$

Here,  $\psi_t$  and  $\theta_t$  correspond to the target azimuth and elevation angles. The target is oriented such that  $\vec{u}_1^{(t)}$  vector is always normal and pointing outward from the sphere surface. Note that this sequence is free from singularity and

This rotational sequence is also known as spherical coordinate system. The resultant transformation matrix between inertial to target CF is as follows:

$$C^{(o,t)} = C^{(o,c)} C^{(c,t)} \quad (34)$$

$$C^{(o,t)} = \begin{bmatrix} c\psi_t & -s\psi_t & 0 \\ s\psi_t & c\psi_t & 0 \\ 0 & 0 & 1 \end{bmatrix} \times \begin{bmatrix} c\theta_t & 0 & s\theta_t \\ 0 & 1 & 0 \\ -s\theta_t & 0 & c\theta_t \end{bmatrix} \quad (35)$$

$$C^{(o,t)} = \begin{bmatrix} c\psi_t c\theta_t & -s\psi_t & c\psi_t s\theta_t \\ s\psi_t c\theta_t & c\psi_t & s\psi_t s\theta_t \\ -s\theta_t & s\rho & c\theta_t \end{bmatrix} \quad (36)$$

Seeker LOS and Seeker Reference frames are constrained to move in roll-nod motion, namely 1-3 Euler rotation sequence and non-singular for  $\eta \neq 0$ :

$$\begin{array}{ccc} \vec{u}_1^{(o)} & \vec{u}_3^{(e)} & \\ \mathcal{F}_o \rightarrow \mathcal{F}_e \rightarrow \mathcal{F}_s & & \\ \rho & \eta & \end{array} \quad (37)$$

$$\begin{array}{ccc}
\overrightarrow{u_1}^{(o)} & \overrightarrow{u_3}^{(f)} & \\
\mathcal{F}_0 \longrightarrow \mathcal{F}_f & \longrightarrow \mathcal{F}_r & \\
\rho_r & \eta_r & 
\end{array} \quad (38)$$

Resultant coordinate transformation matrices are identical to ( 11 )

$$\mathcal{C}^{(o,s)} = \begin{bmatrix} c\eta & 0 & s\eta \\ s\eta \ s\rho & c\rho & -c\eta \ s\rho \\ -c\rho \ s\eta & s\rho & c\eta \ c\rho \end{bmatrix} \quad (39)$$

$$\mathcal{C}^{(o,r)} = \begin{bmatrix} c\eta_r & 0 & s\eta_r \\ s\eta_r \ s\rho_r & c\rho_r & -c\eta_r \ s\rho_r \\ -c\rho_r \ s\eta_r & s\rho_r & c\eta_r \ c\rho_r \end{bmatrix} \quad (40)$$

Recall the assumption made in 2.1 that Seeker Reference CF is always pointing towards the target, seeker-to-target pointing vector can be resolved in inertial CF with seeker reference and target parameters as follows:

$$\vec{r}_{t/s} = |\vec{r}_{t/s}| \overrightarrow{u_1}^{(r)} = \overrightarrow{u_1}^{(r)} \quad (41)$$

$$\bar{r}_{t/s}^{(0)} = \hat{\mathcal{C}}^{(0,r)} \overrightarrow{u_1}^{(r)} = \begin{bmatrix} c\eta_r \\ s\eta_r \ s\rho_r \\ -c\rho_r \ s\eta_r \end{bmatrix} \quad (42)$$

$$\vec{r}_{t/s} = |\vec{r}_{t/s}| \overrightarrow{u_1}^{(t)} = \overrightarrow{u_1}^{(t)} \quad (43)$$

$$\bar{r}_{t/s}^{(0)} = \hat{\mathcal{C}}^{(0,t)} \overrightarrow{u_1}^{(t)} = \begin{bmatrix} c\psi_t \ c\theta_t \\ s\psi_t \ c\theta_t \\ -s\theta_t \end{bmatrix} \quad (44)$$

Equating ( 42 ) and ( 44 ) yields:

$$\bar{r}_{t/s}^{(0)} = \begin{bmatrix} c\psi_t c\theta_t \\ s\psi_t c\theta_t \\ -s\theta_t \end{bmatrix} = \begin{bmatrix} c\eta_r \\ s\eta_r s\rho_r \\ -c\rho_r s\eta_r \end{bmatrix} \quad (45)$$

The solution of above equation is similar to ( 20 ). The target position is input, therefore left-hand side of (46) is all known. Let p represent the L.H.S vector terms in ( 45 ): For  $-\frac{\pi}{2} < \theta_t < \frac{\pi}{2}$

$$\begin{bmatrix} p_1 \\ p_2 \\ p_3 \end{bmatrix} = \begin{bmatrix} c\eta_r \\ s\eta_r s\rho_r \\ -c\rho_r s\eta_r \end{bmatrix} \quad (46)$$

From first row, nod angle of Seeker Reference CF ( $\eta_r$ ) can be calculated with one sign ambiguity as follows:

$$\cos \eta_r = p_1 \rightarrow \sin \eta_r = \sigma \sqrt{1 - p_1^2}, \quad (\sigma = \pm 1) \quad (47)$$

$$\eta_r = \text{atan2}(\sigma \sqrt{1 - p_1^2}, p_1) \quad (48)$$

Using second and third rows of ( 46 ) with ( 48 ):

$$\text{if } \eta_r \neq 0, \quad \sin(\rho_r) = \frac{p_2}{\sin(\eta_r)} \quad (49)$$

$$\text{if } \eta_r \neq 0, \quad \cos(\rho_r) = \frac{p_3}{-\sin(\eta_r)} \quad (50)$$

Using atan2 function yields roll angle of Seeker Reference CF ( $\rho_r$ ) with the same sign ambiguity in ( 48 ):

$$\rho_r = \text{atan2}(\sigma k_2, -k_3), \text{ if } \eta \neq 0, \quad (\sigma = \pm 1) \quad (51)$$

Here, it has to be noted that Target CF has two singularity points at  $\theta_t = \frac{\pi}{2}$  and  $\theta_t = -\frac{\pi}{2}$  where azimuth angle  $\psi_t$  becomes arbitrary. The results show that, zenith location of the seeker ( $\eta = 0$ ) corresponds to the orientation with  $\theta_t = 0$ ,  $\psi_t = 0$  in Target CF which is far away from its singularity point.

### 2.3.2. Angular Velocity Analysis

For a predefined target trajectory as a function of time, the corresponding gimbal reference angular rates can be found by taking time derivative of target pointing vector (46) as follows:

$$\begin{aligned} \frac{d}{dt}(\bar{r}_{t/s}^{(0)}) = & \\ \begin{bmatrix} -c(\psi_t) s(\theta_t) \dot{\psi} - c(\psi_t) s(\theta_t) \dot{\theta}_t \\ c(\psi_t) c(\theta_t) \dot{\psi}_t - s(\psi_t) s(\theta_t) \dot{\theta}_t \\ -c(\theta_t) \dot{\theta}_t \end{bmatrix} = & \quad (52) \\ \begin{bmatrix} -s(\eta_r) \dot{\eta}_r \\ c(\eta_r) s(\rho_r) \dot{\eta}_r + c(\rho_r) s(\eta_r) \dot{\rho}_r \\ s(\eta_r) s(\rho_r) \dot{\rho}_r - c(\eta_r) c(\rho_r) \dot{\eta}_r \end{bmatrix} & \end{aligned}$$

Note that L.H.S. of ( 52 ) and  $\eta_r$ ,  $\rho_r$  are known from previous angular position analysis. The unknowns  $\dot{\eta}_r$  and  $\dot{\rho}_r$  can be extracted by simple algebra.

$$\begin{bmatrix} t_1 \\ t_2 \\ t_3 \end{bmatrix} = \begin{bmatrix} -s(\eta_r) \dot{\eta}_r \\ c(\eta_r) s(\rho_r) \dot{\eta}_r + c(\rho_r) s(\eta_r) \dot{\rho}_r \\ s(\eta_r) s(\rho_r) \dot{\rho}_r - c(\eta_r) c(\rho_r) \dot{\eta}_r \end{bmatrix} \quad (53)$$

Note that there are no additional sign ambiguities in calculating gimbal angular rates.

$$\text{if } \eta_r \neq 0, \quad \dot{\eta}_r = -\frac{t_1}{\sin(\eta_r)} \quad (54)$$

$$\text{if } \eta_r \neq 0, \quad \dot{\rho}_r = \frac{t_2 - c(\eta_r) s(\rho_r) \eta_r}{c(\rho_r) s(\eta_r)} \quad (55)$$

It is clearly seen from ( 54 ) and ( 55 ) that, as the nod angle goes to zero, calculated gimbal rates go to infinity. It is mathematically proven that if the target moves around zenith, direct kinematic inversion will yield infinitely large roll and nod angles.

The angular rate calculations showed that the differential Jacobian of the gimbal gets ill-conditioned near the nadir zone and is rank deficient at the center, proving that infinitely large rate commands will be demanded for finite movements of the target.

#### 2.4. Results of Engagement Loop Analysis

Gimbal is the mechanism which controls the ATTPS's line-of-sight (LOS) for accurate pointing and tracking of the target. Generally, it is composed of a serial manipulator composed of rotary joints mounted orthogonal to each other.

One inherent drawback of the gimbals is that, for specific orientations the LOS vector may align with one of the rotation axes, causing kinematic singularity. If not handled well, it may cause the guidance computer to generate very fast rotary motion commands and loss of target lock-on. In literature, this condition is referred as "gimbal lock", "zenith pass", "nadir", or "keyhole".

It is important to note that, alternative kinematic expressions, like quaternions cannot be employed as a solution since the problem itself is a result of the physical configuration of the target and the gimbal, rather than just an implication of modelling kinematics [14]. The lost degree of freedom is due to kinematics, not notation. Therefore, expressing the problem with quaternions will not yield lower levels of roll rate commands in the nadir cone.

In sections 2.2 and 2.3, target engagement condition is analysed and it is proven that zenith region conditions cause track loss by commanding infinitely large turning rates. In addition, zenith pass yields infinitely many solutions. The susceptible region for ZP problems highly depends on other ATTPS parameters.

## **2.5. Critical ATTPS components affecting tracking performance**

This section is devoted to a deeper analysis on ATTPS. The aim is to provide a deeper insight to the reader on ATTPS components, before Chapter 3 in which a detailed simulation model is constructed.

### **2.5.1. Field of View and Field of Regard**

Field of view (FOV) is defined as the imaging cone that the seeker has at a specific gimbal orientation. LOS vector determines the centerline of this imaging cone. The angle of this cone has a critical importance in mission planning. A larger cone angle yields a wide imaging area, which eventually limits detection range. A narrow one, however, yields a larger range but suffers from small imaging area. The FOV angle should be selected according to the target maneuver capability.

Field of regard (FOR) is defined as the solid angle which can be scanned by IIR imager with the help of gimbal. Having a wide FOR is critical to provide a larger engagement zone.

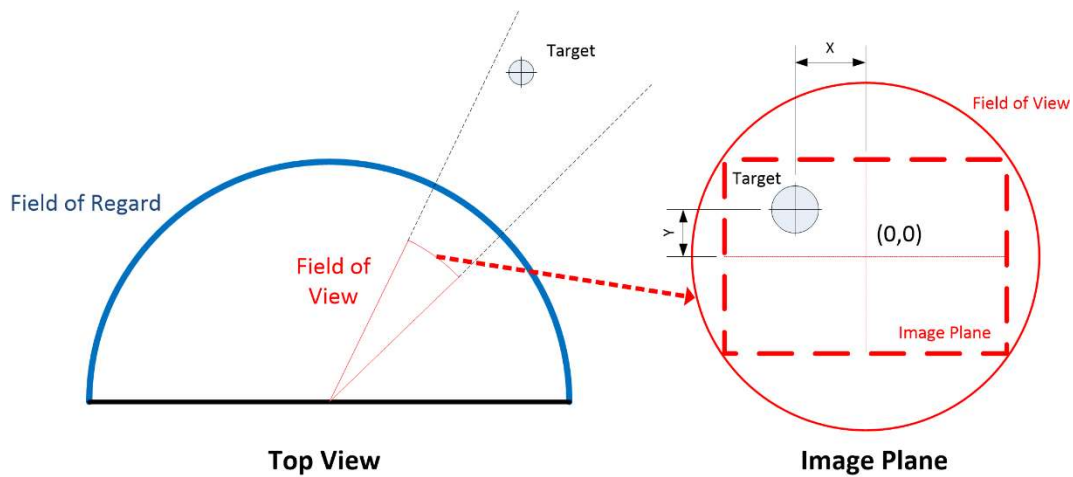


Figure 2.2. Field of View and Field of Regard

The concept is illustrated in Figure 2.2. Here, an imaging system with hemispherical FOR is depicted. At the instant, target lies inside the image plane therefore can be tracked by tracker algorithm.

It is common in gimbals that the cone including zenith and its neighborhood is cut out from the center of FOR as a method of avoiding singularity. Although being practical, it is an incomplete solution since track loss due to wild roll gimbal rates near zenith is still unavoidable.

Due to the kinematic constraints, pitch-yaw configured gimbals tend to have smaller FOR ranging around  $\pm 65^\circ$ . In modern air to air missiles like IRIS-T and AIM 9X, FOR goes beyond front hemisphere ( $> \pm 90^\circ$ ) in exchange for having a potential ZP problem in the center. Although this choice brings its own disadvantage, system designers tend to use roll-nod gimbals to achieve a larger envelope to launch the missile [15].

The second important parameter is FOV, which is determined by the optical design of the camera carried by the gimbal. A narrow FOV leaves a little room for tracker to compensate for the instantaneous off-boresight error. It is possible to state that,



FOV puts a limit on allowable error budget for target tracking and has to be considered carefully during system design.

### **2.5.2. Target Manoeuvrability**

Agility of the target is another important parameter in ATTPS design. As formulated in section 2.3, LHS of equation ( 52 ) linearly increases with observed target angular rates. As the engagement gets close to zenith, resultant gimbal rates tend to infinity.

The engagement of a fighter aircraft and an air-to-air missile equipped with a gimballed seeker is a good example of agile maneuvering scenario. There are numerous studies to find the optimal motion and timing for each side of this duel. For the aircraft, evasive maneuvers like High-G Barrel Roll, Split-S and Vertical-S are few examples [16]. On the other hand, missile navigation and guidance rules are optimized every day. This is a never-ending race where one side is running, and the other side is chasing.

Turning back our focus to ATTPS, the problem can be mapped to the gimbal in terms of maximal angular rates that can be demanded during a scenario. In the upcoming simulation phase of this study, some realistic assumptions will be made on that value. The achievable angular rate directly affects the size of zenith cone.

### **2.5.3. Gimbal Rate Limit and Controller**

Among the ATTPS sub-systems explained so far, gimbal controller has a very critical role. Its rate limit and bandwidth should be compatible with the fastest expected command, defined as target maneuverability in the previous section.

Gimbal controller has the fastest sampling time and highest bandwidth among other sub-systems related to target tracking. Therefore, it is important to keep its bandwidth at a certain level, in other words, provide a smooth, flat bode plot for each axis.

Structural rigidity is an important issue covered in ATTPS design. Gimbals especially for mission critical applications, are highly linear. So, with a proper

mechanical design and well tuning, it is possible to simplify the 2-axis gimbal control task by splitting into two single axis systems. Each axis can be controlled independently and cross-coupling terms can be regarded as external disturbances.

The ideal control topology for each gimbal axis is presented in Figure 2.3. Here, the tracker generates angular rate commands to the inner loop of the cascaded gimbal controller. The gimbal frame is assumed to have a much higher bandwidth compared to engagement frame, consequently modeling the gimbal and satisfying a certain bandwidth is critical.

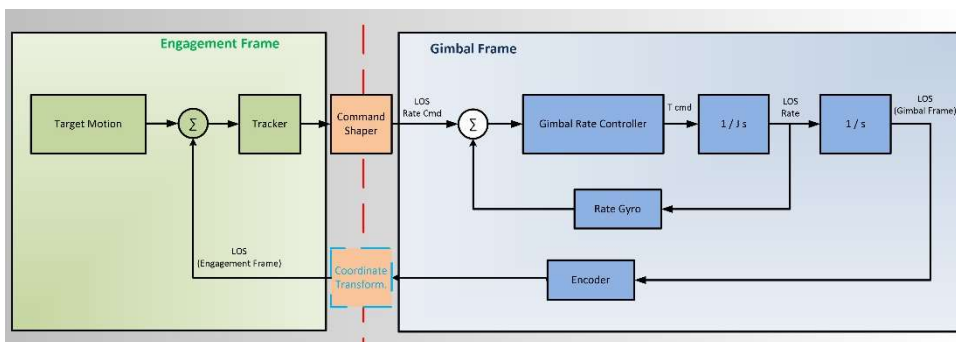


Figure 2.3. ATTPS Control Topology

#### 2.5.4. Tracker

Tracker is basically an image processing and command generation unit working in tandem with gimbal. It works on an image frame which is illustrated on the R.H.S of Figure 2.2. Its aim is to keep the target at the image center, in other words keeping the errors X and Y at zero. Due to the kinematic relations explained in Section 2.3, a straight motion along image plane may cause rotations in both roll and nod axes.

As one might have guessed, it is a discrete system and discretization interval is mainly dependent on the camera's imaging frequency. The tracker handles following tasks periodically at each frame time

- Acquire the last image from the camera
- Discriminate the target from background and identify it

- Calculate necessary gimbal rate commands to keep the target in FOV center.

It is important to complete the above task within a specific time interval delay. This value is called tracker delay and has critical importance in ATTPS design.

The tracker output could be angular position or angular rate depending on the specific system needs. In this work, the focus is primarily on fast steering nod-over-roll configured gimbals, therefore rate-commanding trackers are preferred as in [14].



## CHAPTER 3

### SYSTEM MODEL AND ENGAGEMENT SCENARIOS

In Chapter 1 and Chapter 2, the intended gimbal configuration (nod-over-roll) and its zenith pass problem is explained in detail. Now, the simulation environment and the test scenarios that are built up for studying zenith pass algorithms are explained in detail.

As explained previously, ATTPS design is a multi-disciplinary act and ZPA lies at its core. The approach in this study is to build an ecosystem enveloping ZPA and representing each and every significant sub-system in ATTPS design. The proposed simulation environment allows regression analysis with respect to the critical system parameters given in section 2.5 therefore allows in-depth performance evaluation of the ZP algorithms.

It has to be noted that the simulation is based on the assumptions made in section 2.3, an engagement condition where the gimbal is fixed, and the target motion is mapped to a unit circle around.

#### **3.1. Simulation Model**

An overview of the simulation model is shown in Figure 3.1. It is mainly composed of three sub-systems:

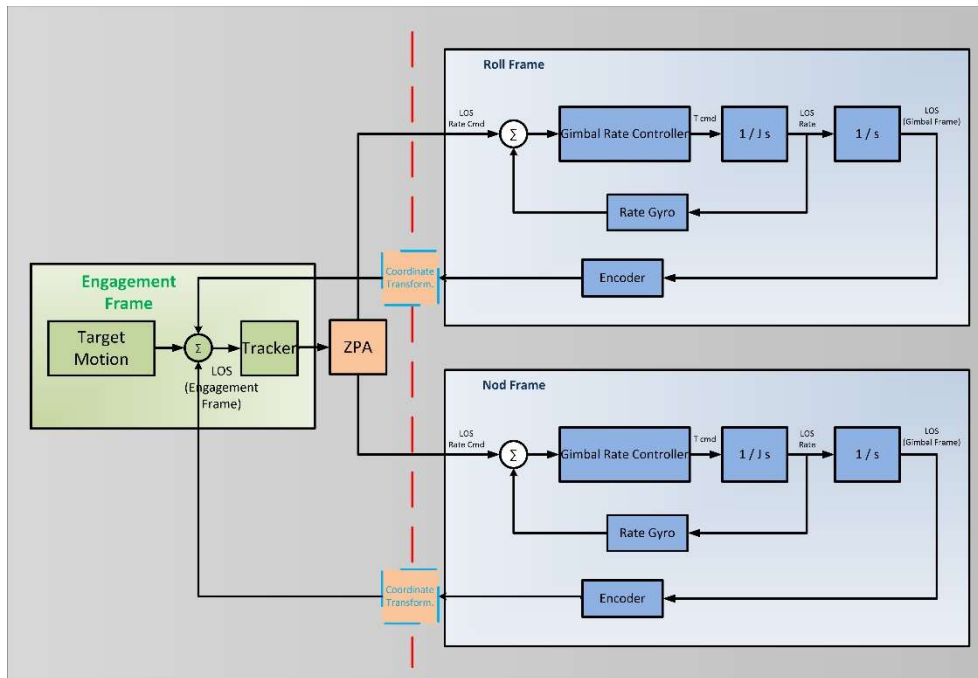


Figure 3.1. System Block Diagram

From left to right, the first system is the engagement frame where the input (target location) and image tracker operates. The target location and transformed gimbal LOS are compared, calculated LOS error is fed to the tracker and it generates necessary rate commands in the singularity free azimuth-elevation frame.

Secondly, the intermediate blocks including Zenith Pass Algorithm, shapes the tracker commands and maps them into nod-over-roll gimbal frame.

Lastly, RHS of the block diagram shows independent roll and nod controllers. They receive shaped rate commands from ZPA and try to realize them. The closed-loop bandwidth of gimbal controllers are set to higher values than that of tracker, avoiding any kind of interaction.

The overall structure of the simulation is composed of two cascaded loops. The inner loop is composed of a high bandwidth gimbal control system that is responsible from realizing the provided roll and nod angle rate commands that are generated by the tracker and re-shaped by the ZPA.

The outer loop is formed by the combination of the tracker and ZPA. This outer loop receives the target location as command and the gimbal states as feedback. With necessary coordinate transformations, tracker generates a rate command for the gimbal in the singularity free reference frame. This is followed by ZPA which reshapes the command to nod-over-roll frame while catching the onset of ZP depending on the selected algorithm mode. The system is realized on MATLAB SIMULINK environment. An overview of the top-level simulation file is given in Figure 3.2

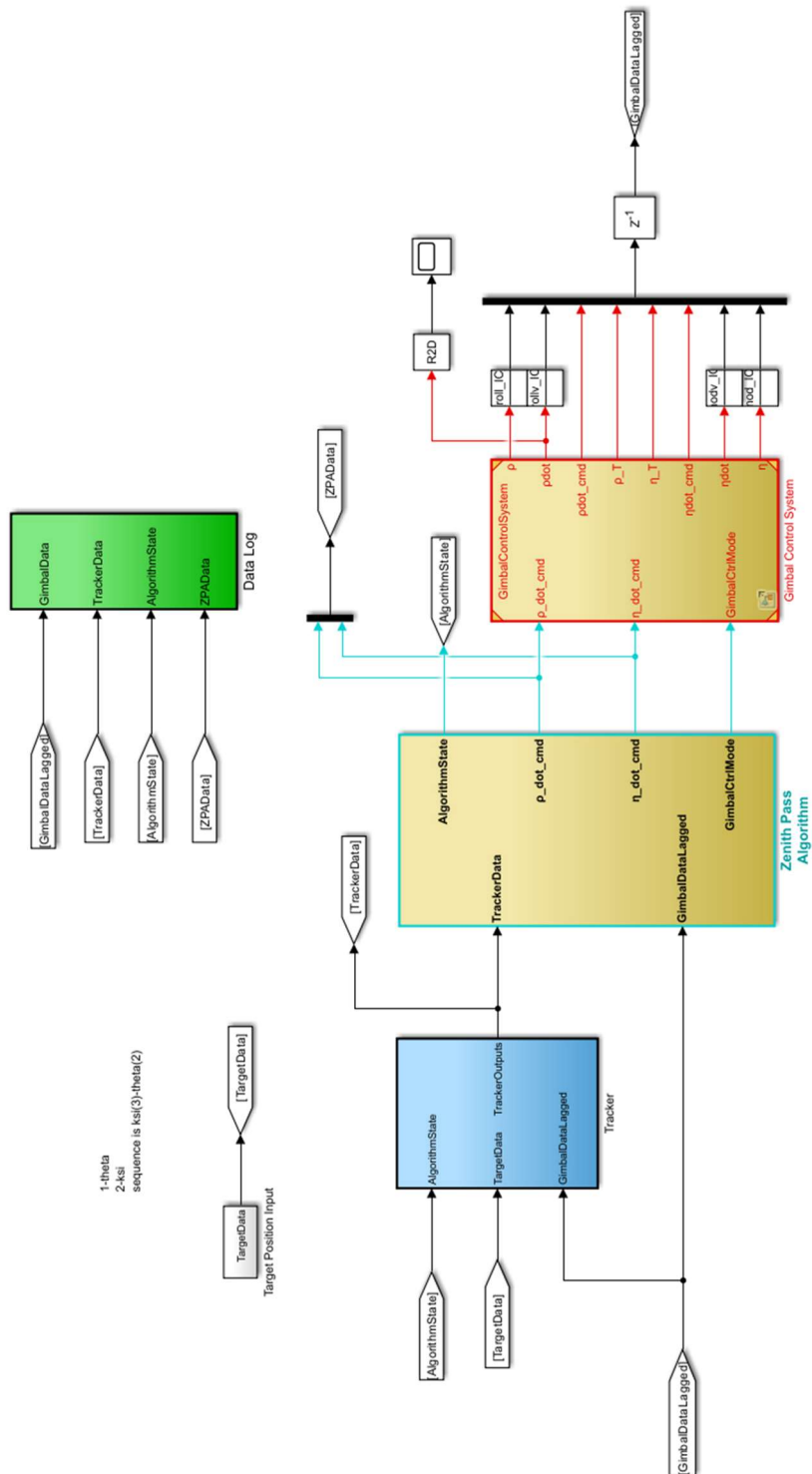


Figure 3.2. Simulation Overview



### 3.1.1. Gimbal and Control System Model

The generic EOM for each rotating gimbal axis can be written in body fixed frame as follows:

$$\hat{J}_b \dot{\bar{\omega}} + \bar{\omega} \times \hat{J}_b \bar{\omega} = \sum T \quad (56)$$

The roll-over-nod gimbal has 2 DOF and is equivalent to an RR type serial 2-axis robotic manipulator. Due to misalignments, unbalanced inertia terms (off-diagonal elements in J matrix) and base movements gyroscopic terms are inevitable.

Note that the gyroscopic term in above equation ( $\bar{\omega} \times \hat{J}_b \bar{\omega}$ ) disappears for roll axis in the unit sphere approach. However, the movement of roll axis still creates a gyroscopic term on nod, and nod axis will exert reaction forces appearing as disturbance torque on the roll axis. The level of aforementioned disturbances significantly dependent on the inertia tensor  $\hat{J}_b$ , therefore omitted.

It is shown that, even this simplified 2-axis gimbal model includes significant amount of nonlinearities[17]. However, they are all negligible when compared to the inertial term. For the sake of simplicity, each gimbal axis will be modelled as single DOF systems. Such decoupling in gimbal axes is referred as decentralized control. [4][18] The cross-coupling terms are omitted.

$$I\ddot{\rho} + D\dot{\rho} = \sum T_{roll} \quad (57)$$

$$I\ddot{\eta} + D\dot{\eta} = \sum T_{nod} \quad (58)$$

Note that there are no stiffness terms in the EOMs. This is primarily due to the fact that in ATTPS gimbals, axes are well designed to minimize friction, unbalance and resistance to rotation. The roll axis is free to rotate without limit and the nod axis has

only negligible amount of cable restraint torque. So, it is safe to assume that only inertia and a viscous damping terms exist. The basic models for roll and nod axes are illustrated in below figure:

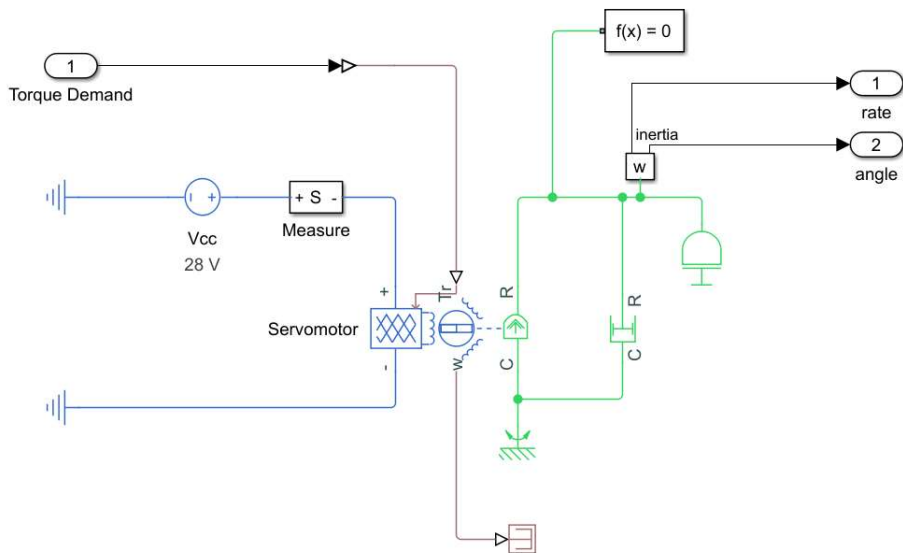


Figure 3.3. Roll and Nod Gimbal Models

The inertia and viscous damping values are selected to be the same for each axis. Normally, kinematic parameters of the outer axis should be significantly larger compared to the inner. Although this seems contradictory, the logic behind this simplification is to achieve a specific closed loop control bandwidth for each axis with minimum effort.

From ZPA design point of view, the only important feature of gimbal models are their fidelity and closed loop bandwidth. The physical properties (inertia, damping, motor torque etc.) of roll and nod gimbals are irrelevant in terms of ZPA development. Therefore, it is possible to use the same plant model for both roll and nod axes, which halves the workload of tuning gimbal controllers.

As explained in section 2.5.3, gimbal controller bandwidth is one of the most important parameters within the scope of this analysis. Physical values of inertia,

damping and omitted friction values do not contribute to the result as long as a specific control bandwidth is achieved.

The Gimbal Control System is responsible from simulating both the gimbal dynamics and gimbal controller behaviour. The block diagram of the overall control system is given below:

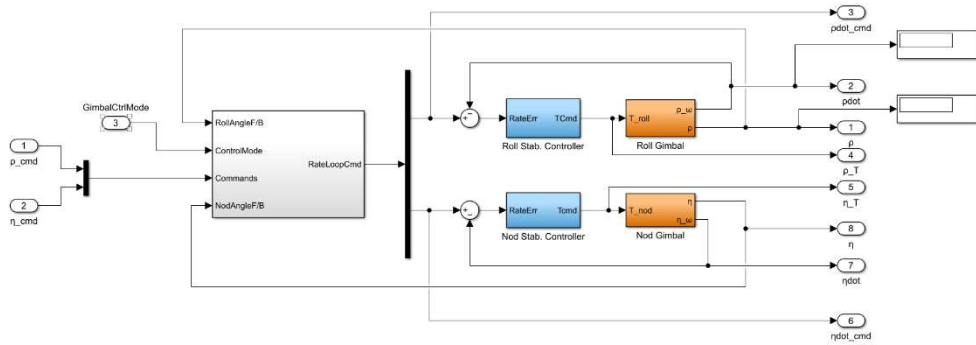


Figure 3.4. 2-Axis Gimbal Control Model

As explained before, the gimbals are modelled as two identical single-DOF systems. Therefore, their controllers are modelled as classical PID type SISO systems, achieving predefined bandwidth values.

Most of the ATTPS include a set of cascaded control configurations enabling the user to control either angular position or angular rate of the gimbal. The scope of this study necessitates only rate controller, therefore for the sake of simplicity, a set of rate loop controllers are designed parametrically.

The plant for the rate loop is a low pass filter in the following form:

$$G_{p\ rate} = \frac{1}{I_{nod} + d_{nod}} \quad (59)$$

As shown in above equation, the plant has no free integrators. In order to have a Type II response in closed loop, a double PID is selected as control method. It basically

includes double integrator and double zeros on the complex plane. The form of the controller is given below:

$$G_{C\ rate}(s) = \frac{K_p(s + a)(s + b)}{s^2} \quad (60)$$

The rate controller is designed in MATLAB Control System Designer with the plant and controller form given in (59) and (60). A capture taken from the design process is given below.

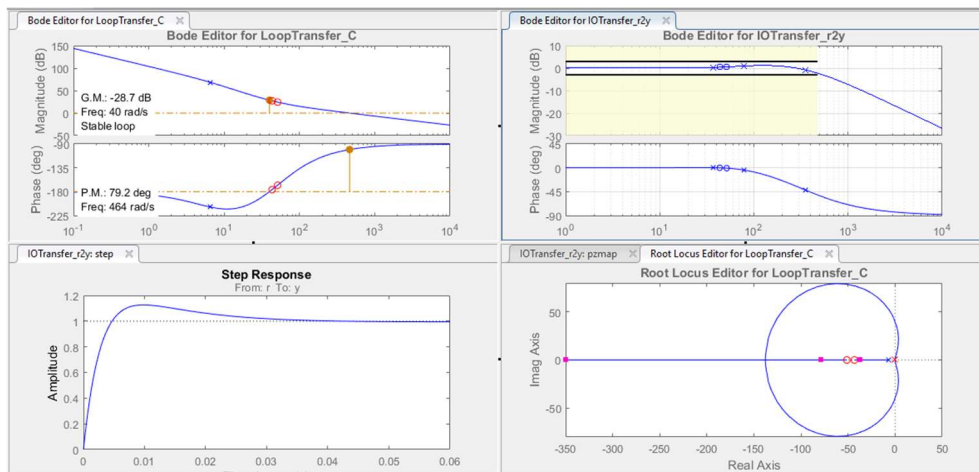


Figure 3.5. Rate Loop Controller Design

The concept is realized by designing different gimbal controllers. It is possible to switch the controllers from command line, and vary the closed loop bandwidth of both roll and nod axes in a large range from 1 Hz to 60Hz. This enables to study ZPA performance with respect to gimbal rate controller bandwidth.

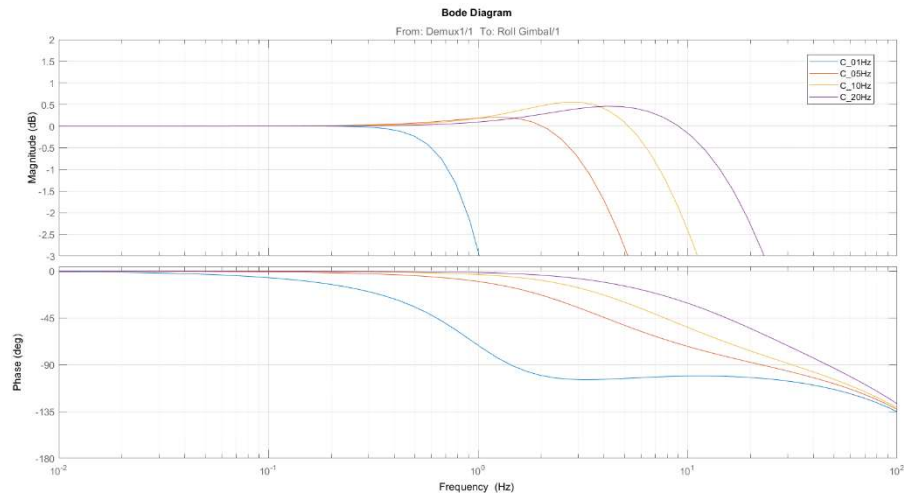


Figure 3.6. Closed Loop Bode Diagrams of Some of the Tuned Rate Controllers

Gimbal plant is constructed via SIMSCAPE<sup>®</sup> and isolated from the rest by “model referencing”. This choice made it easier to tune the stabilization controller from command line. In a separate file dedicated for bandwidth tuning, the same gimbal plant is operated with the PID controller in a feedback loop, and tuned by SIMULINK<sup>®</sup>. The close loop bode diagrams of some controllers are given in Figure 3.5.

The operating frequency of the model is selected as 2kHz. Note that the sampling interval is at least 18-times higher than the highest controller bandwidth (60Hz) which eliminates any kind of discretization errors.

### 3.1.2. Target Tracker Model

The outline of target tracker and its role in ATTPS was expressed in Section 2.5.4. For studying ZPA, it is crucial to have a realistic target tracker creating necessary commands. Now, the specific modelling effort will be explained in detail.

In this case, the dominant tracker behaviour is a pure delay of several multiples of frame time. [19] It has to be underlined that this approach assumes that tracker

always process the image and return the target location with a high confidence. In short, the stochastic nature of image processing is omitted in the simulation.

Tracker utilizes sophisticated video/image processing algorithms to detect, identify and track the target during operation, which is beyond the scope of this work. In this study, tracker will be modelled ideally by considering some of its primary parameters affecting ATTDS performance.

Its main aim is to process the target image obtained from the optics located on gimbal and create reference commands for gimbal to rotate. All the work related to singularity handling is left to ZPA, therefore tracker is assumed to work in a singularity-free coordinate frame, which is similar to the approach in [12].

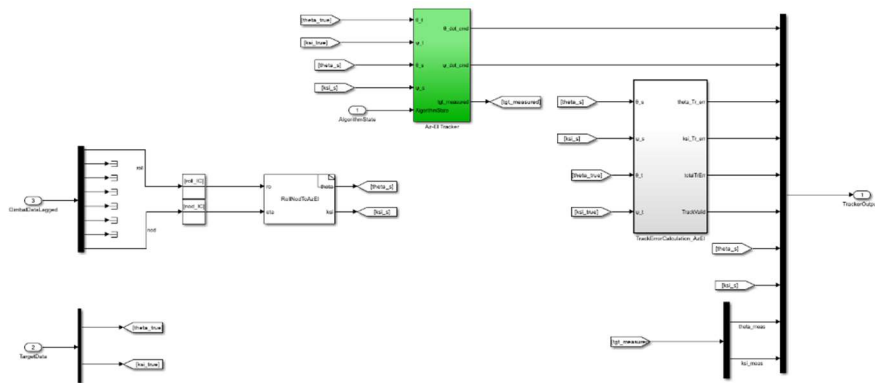


Figure 3.7. Tracker Block Diagram – Top Level

To do this, the gimbal feedback taken in roll-nod frame must be converted into azimuth-elevation frame at the entrance. This is done by solving the L.H.S. of ( 45 ). Unlike the approach in Section 2.3.1, equation is solved for  $\psi_t$  and  $\theta_t$  this time.

The gimbal angles are input, therefore R.H.S. of ( 45 ) is all known. Let r represent the R.H.S vector terms in that equation. For  $-\frac{\pi}{2} < \theta_t < \frac{\pi}{2}$  :

$$\begin{bmatrix} r_1 \\ r_2 \\ r_3 \end{bmatrix} = \begin{bmatrix} c\psi_t c\theta_t \\ s\psi_t c\theta_t \\ -s\theta_t \end{bmatrix} \quad (61)$$

From first and second rows, gimbal orientation in tracker reference CF can be calculated without sign ambiguity as follows:

$$\psi_t = \text{atan2}(r_2, r_1) \quad (62)$$

$$\theta_t = \text{atan2}\left(-r_3, \frac{r_2}{s\psi_t}\right) \quad (63)$$

The formulation is realized right at the entrance of Tracker subsystem as shown in Figure 3.7.

As explained in section 2.5.4, rate commanding tracker scheme is preferred. This design choice showed itself as a control problem in which the plant is a pure integrator.

Naturally the tracker is a sampled device operating with a sequence of images, on which the target coordinate is sought dynamically with respect to image center. This computational effort brings an inevitable phase delay to the track loop, which is called image processing delay.[20]

In this simulation, fundamental imaging frequency is selected as 100 Hz, and image processing delay is taken as 2 frames long. Those values are determined from literature by considering similar ATTDS system properties. [1] They are reflected to the SIMULINK model with proper sampling, delay and rate transition blocks.

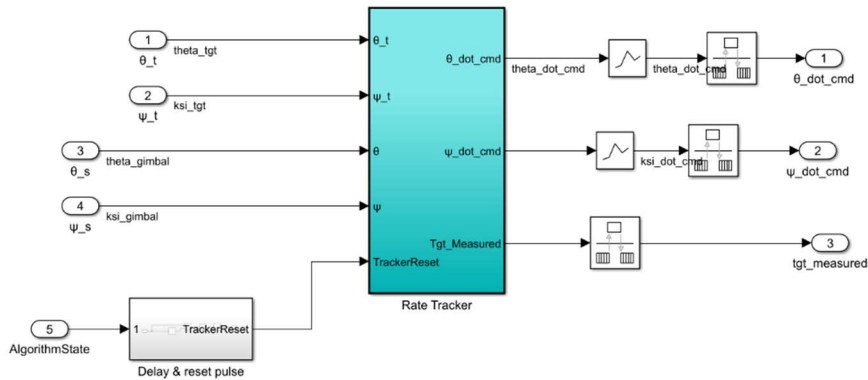


Figure 3.8. Rate Tracker – Middle Level

Nonetheless, the image processing delay causes a significant phase lag, therefore the linear automated controller tuning methods used in gimbal controller cannot not be implemented here. Tracker is manually tuned to achieve a bandwidth of 5Hz which is far enough from gimbal controller bandwidth to avoid any kind of interaction.

The tracker block runs at 100 Hz, which is the assumed imaging frequency. Figure 3.8 shows the up-sampling of tracker calculations to 2kHz, which is the real-time gimbal controller operating frequency.

depicts the innermost level of the tracker in which, image quantization error, image processing delay and line of sight errors are calculated. The tracker generates rate commands in azimuth-elevation frame and feeds outwards.



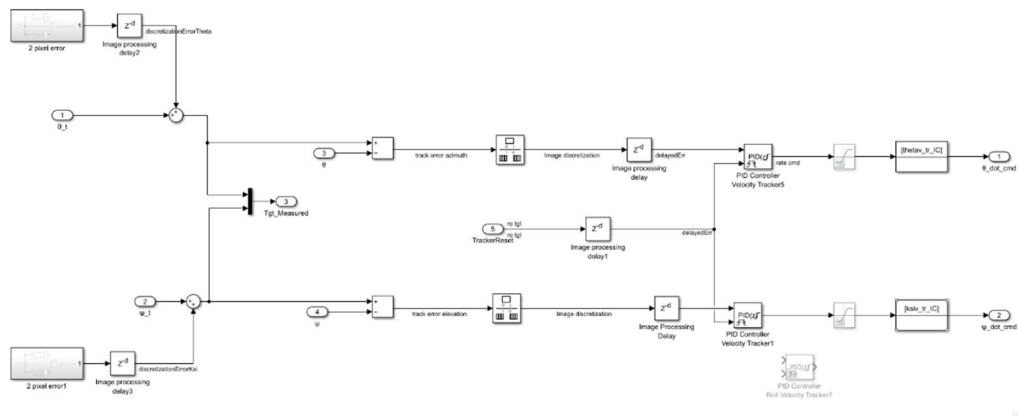


Figure 3.9. Rate Tracker – Bottom Level

The camera optics play an important role while extracting commands from image pixel data. If reflective elements are utilized in the optical design, image might rotate on the focal plane and has this rotation has to be compensated at each frame as a function of instantaneous gimbal angles. The author has conducted a detailed analysis on an exemplary gimbal with reflective optics [12]. For further information, the reader may refer to that source. In this work, however, the focus will be solely on ZPA design.

The primary tracker tasks, namely image processing and target state estimation are beyond the scope of this thesis. An idealized behaviour with realistic dynamic properties (image processing delay, quantization errors etc.) are modelled and included in the simulation as parameters.

A brief explanation of tracker subsystem would be as follows: First of all, the target angles expressed in spherical coordinates (3-2 rotation sequence) are fed to the tracker block. This data is delayed for 0.02 sec and down-sampled to 100Hz resembling “visual servoing delay” [1] and image processing time respectively. Resultant target position is fed to the ZP algorithm in the same singularity-free coordinate frame. The delayed off-boresight error can be regarded as the output of the image processing algorithm.

For imitating the tracker behavior, the block observes gimbal states and checks the track loss condition with respect to the following criterion:

- LOS error should be less than half of the FOV
- Gimbal angular rate should be less than the rated value

In a realistic ATTPS configuration, system would lose its target tracking ability if any of the two conditions hold. This is controlled by a logic and in the event of track loss, simulation stops. This control is important to assess ZPA performances in simulation runs.

The last important feature of Tracker Subsystem is monitoring the angular error between the target and Seeker LOS vector during simulation. It is used to check whether the seeker achieves its primary goal, namely keeping the target within its field-of-view (FOV), or not.

For the seeker to function properly, it has to keep the target within its FOV at all times. Due to the dynamic nature of engagement, it is highly unlikely for seeker to find the target again, once it gets out of its sight. At any instant, having the LOS error more than half of the FOV means that the parameter “Acquire Flag” is set to zero and simulation fails. It serves as a sanity check for the entire simulation.

In certain circumstances, this Acquire Flag can be overridden by a clever algorithm estimating the target states for a short duration. Especially in the proximity of zenith cone, such a preemptive action would be useful.

### **3.1.3. Zenith Pass Algorithm**

The zenith pass algorithm block serves as a mapping between tracker and gimbal. Rate commands generated in azimuth-elevation (3-2) sequence is mapped into nod-over-roll (1-3) sequence in this section. This mapping is a common task; therefore, it is placed in every ZPA implemented.

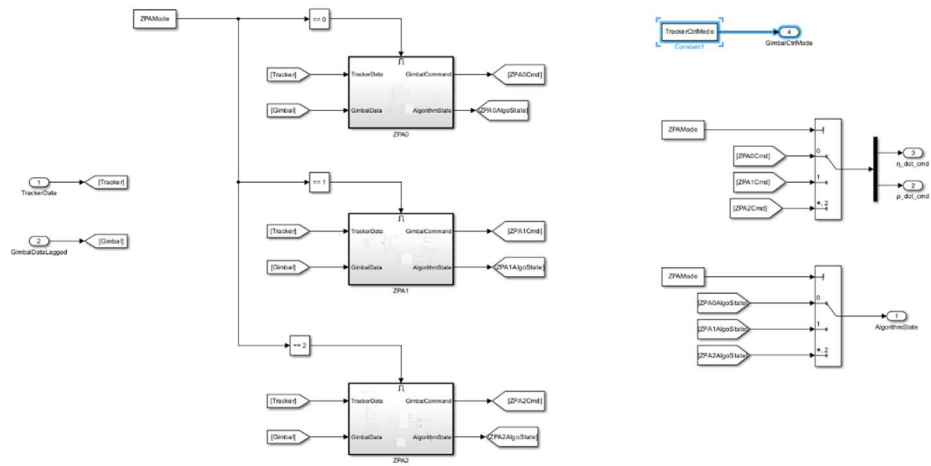


Figure 3.10. ZPA – Top Level

There are three distinct ZPA's in the simulation. Yet, the common aspects will be investigated here. As mentioned earlier, pure inverse kinematics is used for the zone outside zenith.

The inverse kinematics block simply calculates ( 54 ) and ( 55 ) to find roll and nod rates. Note that, azimuth and elevation rate inputs are fed by tracker in the singularity free azimuth-elevation frame. (See Figure 3.11)

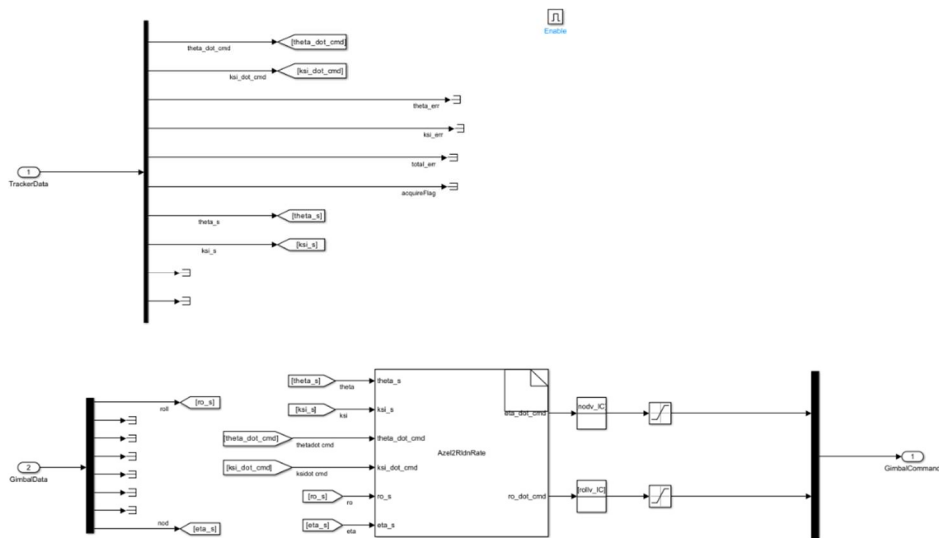


Figure 3.11. ZPA Bottom Level: ZPA0 Kinematic Inversion

ZPA0, which is intended to be the baseline algorithm, solely includes above inverse kinematics calculation. Apart from that, there are 2 more ZP algorithms in this study (ZPA1 and ZPA2) Relying on a logic tied to nod angle, they incorporate different algorithms to handle near-zenith conditions, details of which are explained in Chapter 4.

### 3.2. Exemplary Scenarios

Generating exemplary scenarios for ZPA evaluation is a key part of this modelling work. Sufficient number of simulations with diverse engagement kinematics are needed to validate each ZPA.

During the study, the literature on air-to-air missile engagements was investigated and most common evasive manoeuvres were listed as vertical-s, split-s and barrel-roll.[16] Depending on the initial conditions, (time to go, initial attitudes, etc.) a zenith pass condition may occur during the flight.

With the aim of generating realistic exemplary scenarios, it was decided to conduct a number of simulations in 3-D space involving a pursuer with PNG law and a point-mass target doing predefined evasive manoeuvres. Missile trajectories were the outcome of this analysis, in which seeker gimbal positions and rates are given implicitly. Among them, only limited number of simulations exhibit Zenith Pass problem. Even though a lot of effort was put on generating realistic A2A scenarios, it did not yield sufficient complexity for ZPA algorithm testing. Therefore, it is decided to keep this data aside for further academic work, and continue with synthetic zenith pass scenarios.

Utilizing the experience from realistic air-to-air combat simulation, several synthetic zenith-pass test scenarios are generated. They will be used to evaluate the effectiveness of each ZPA. In designing scenarios, the offset to the zenith is varied gradually. The determined scenarios represent the passage from the zenith point with a certain distance. In their current form, they are a compelling set of scenarios for gimbal control, but the number of theoretically possible engagement conditions is endless. For this reason, it is not appropriate to claim that the selected scenarios are optimal. However, they represent compelling engagement situations for a realistic air-to-air engagement problem.

For each scenario, first the path of the target is defined in the singularity-free task-space (Azimuth-Elevation frame) where the center point corresponds to zenith. Later corresponding joint space (gimbal) trajectories with respect to time are calculated and stored.

Note that when the target passes close to zenith, abrupt increases in roll and nod rates are seen in some of the trajectory plots. Each scenario has a close-zenith or exact zenith-pass condition to test algorithm performance.

It is also important to note that some of the test scenarios (Scenario 4 and 5) are developed to verify the performance of the proposed algorithm on certain problematic operating conditions, rather than performance assessment. For example, a tangent pass from the zenith circle may trigger the algorithm and cause some

unwanted behavior, which has to be adequately filtered. Alternatively, a target might go inside the zenith zone and stay there till the end of the simulation. In that case, the algorithm has to be salient and not yield wild motions.

### **3.2.1. Scenario 1**

Scenario 1 corresponds to the exact zenith pass condition, where the kinematic inversion formula commands nod axis to slew through zenith with no roll rate. However, when the tracker measurement noise is added during the simulation, even infinitesimal changes along the path may yield abrupt changes in the IK solution. The robustness of the algorithms to those possible spikes in rate commands will be examined.

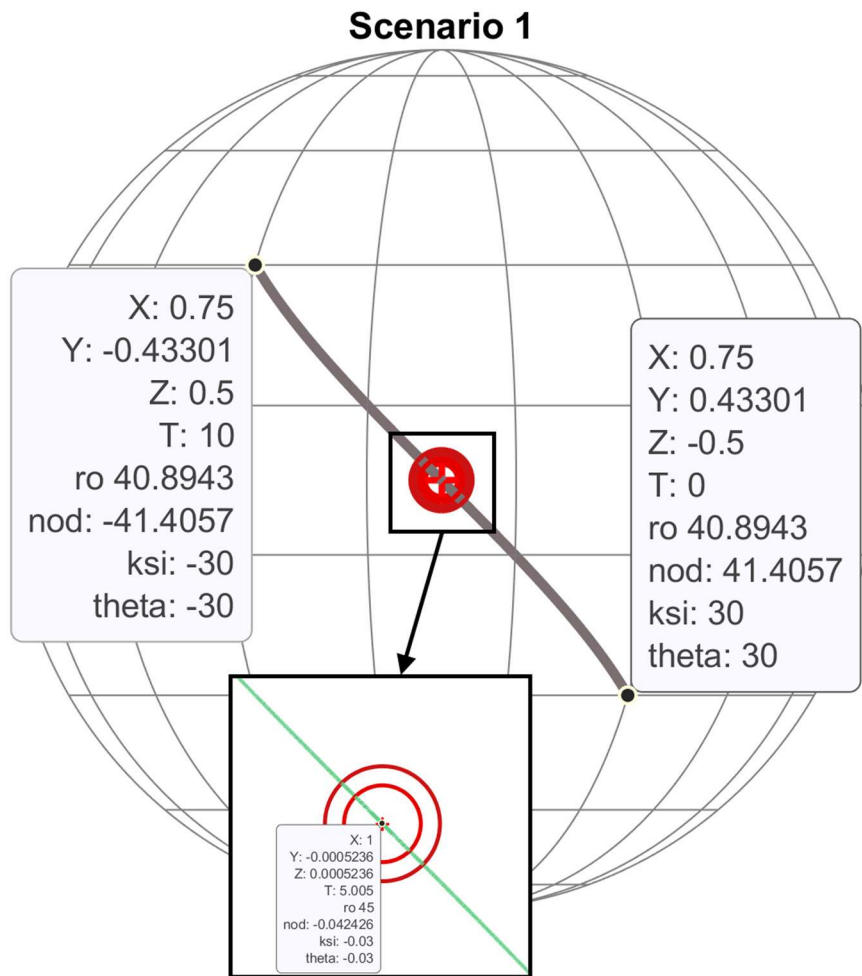


Figure 3.12. Scenario 1 – Path 3D View

Figure 3.12 depicts the trajectory on a unit sphere where the center point corresponds to the zenith. Corresponding task space and joint space variables are presented in the following figure. Although the IK solution eliminates the double-valuedness problem, the scenario is prone to saturation with infinitesimal noise in measurements.

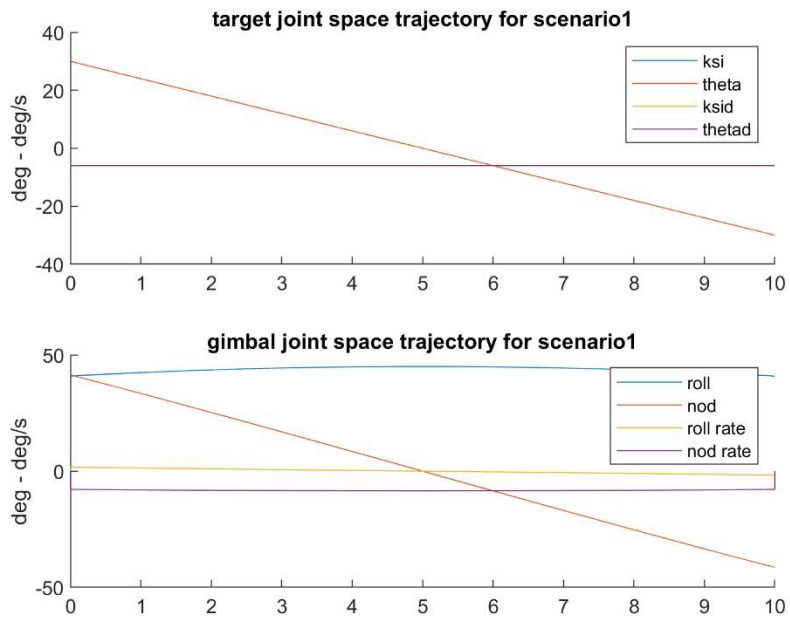


Figure 3.13. Scenario 1 - Trajectories

### 3.2.2. Scenario 2

Scenario 2 represents a close-zenith pass condition where the trajectory is offset from zenith approximately 0.7 degrees.



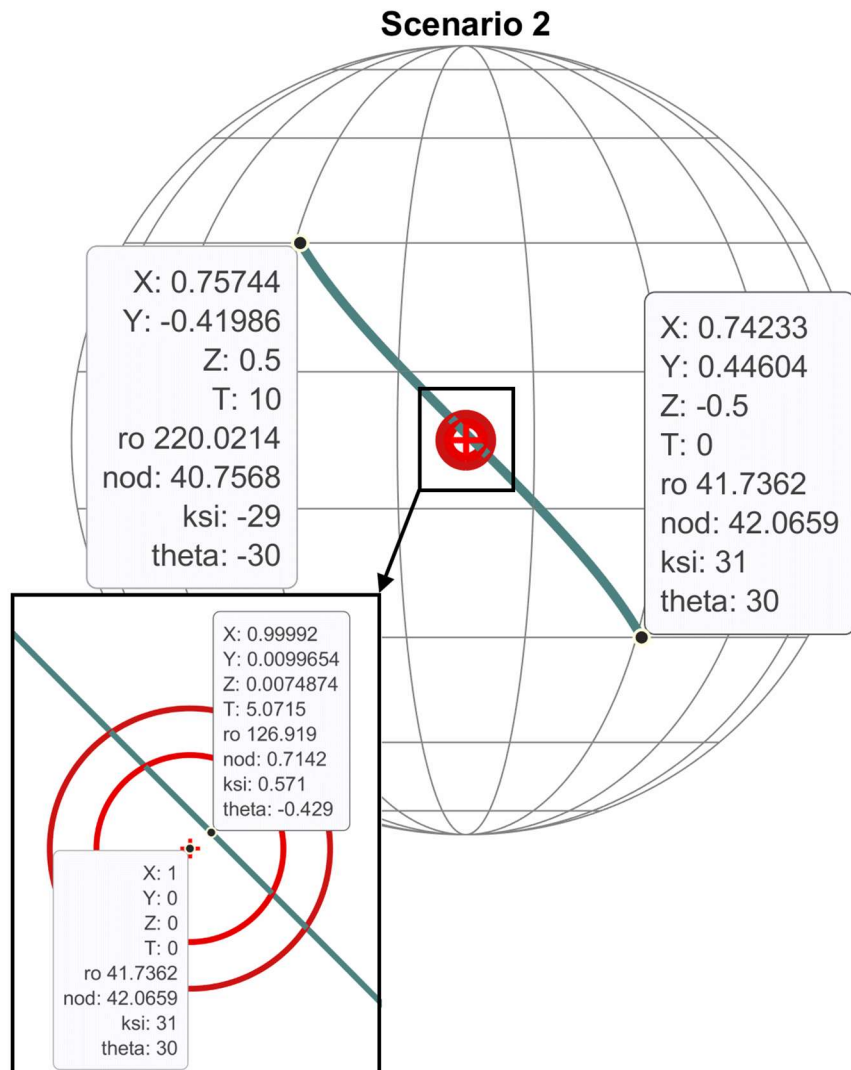


Figure 3.14. Scenario 2 – Path 3D View

Inverse Kinematics solution yields a spike in the roll axis as depicted in below figure.

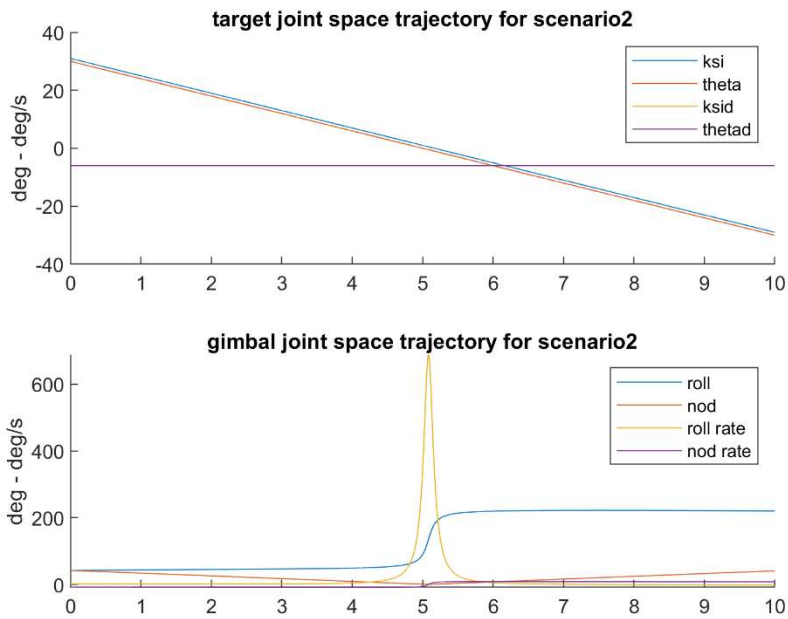


Figure 3.15. Scenario 2 - Trajectories

### 3.2.3. Scenario 3

Scenario 3 represents a far zenith pass condition, where the offset value is 1.4 degrees. Although it yields minimal roll rates compared to other scenarios, Scenario 3 intended to test the discrimination logic of the ZPA's. The algorithm should be able to discriminate far zenith-pass conditions and should not allow for an increased error.

If the ZPA has a poorly designed logic, a far-zenith trajectory may trigger preemptive actions that worsen the tracking performance rather than improving it.

Scenario 3

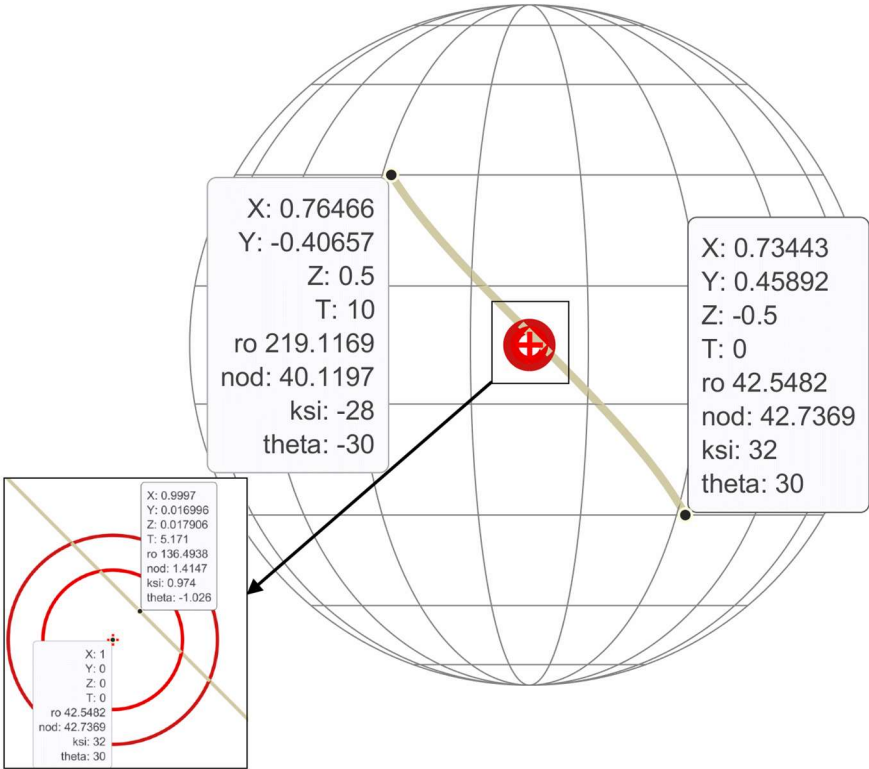


Figure 3.16. Scenario 3 – Path 3D View

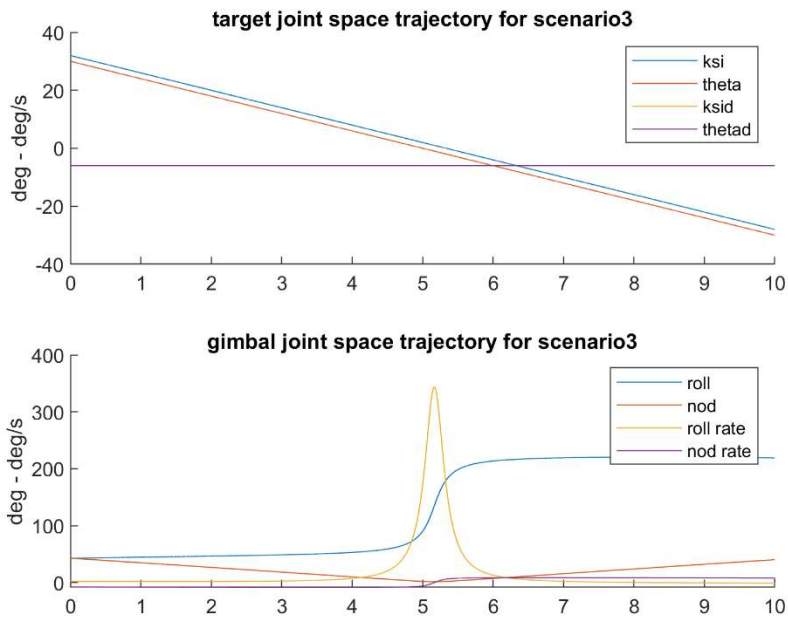


Figure 3.17. Scenario 3 - Trajectories

### 3.2.4. Scenario 4

Scenario 4 is designed to be a sanity check for the proposed algorithm by instantly triggering it with a tangent pass through the zenith circle. A successful algorithm is expected to discriminate such moves and foresee that a zenith pass will not occur. This should lead to the use of IK rather than invoking the estimator.

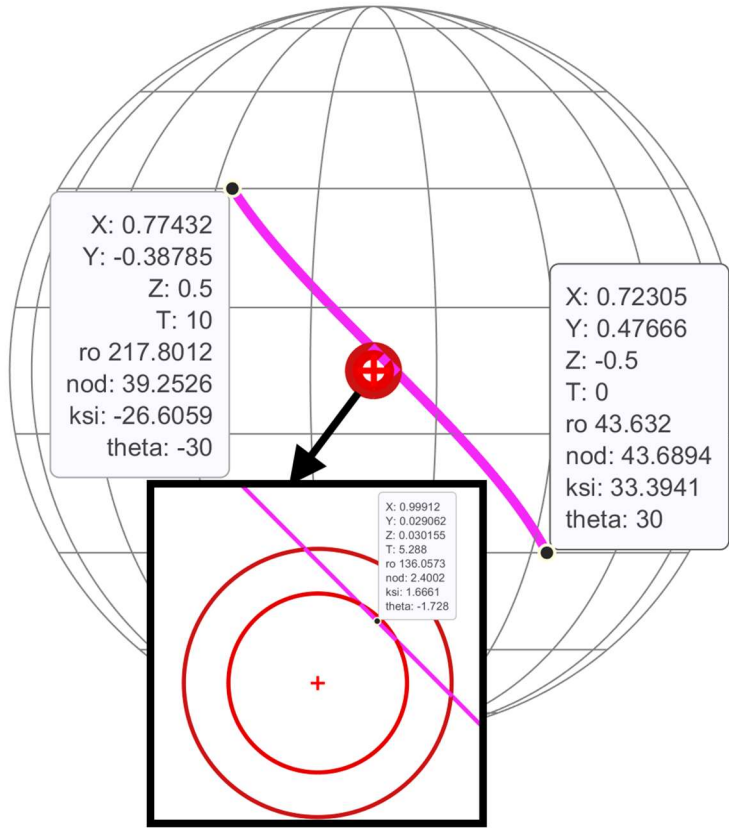


Figure 3.18. Scenario 4 – Path 3D View

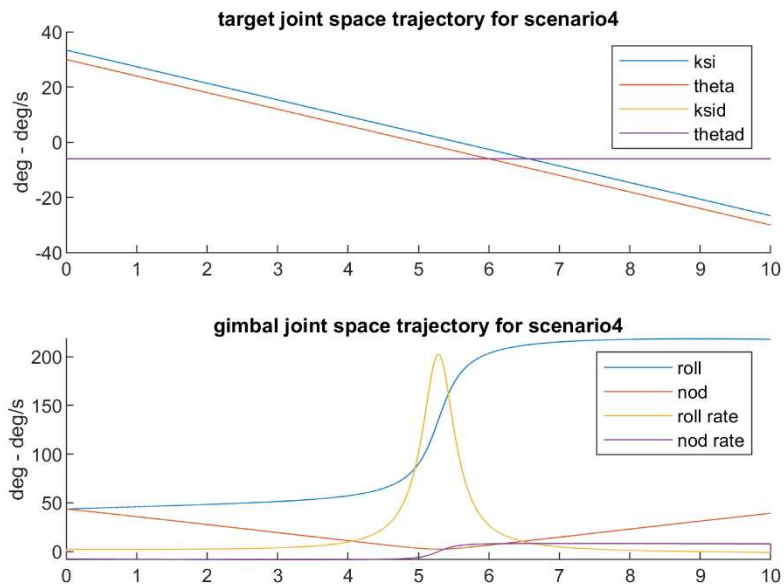


Figure 3.19. Scenario 4 - Trajectories

### 3.2.5. Scenario 5

Scenario 5 is the second sanity check for the proposed algorithm by slowing down the target after going inside zenith circle, and keeping it there with mild motions. A successful algorithm is expected to capture this behavior and do not throw the gimbal to the opposite side of the zenith circle.

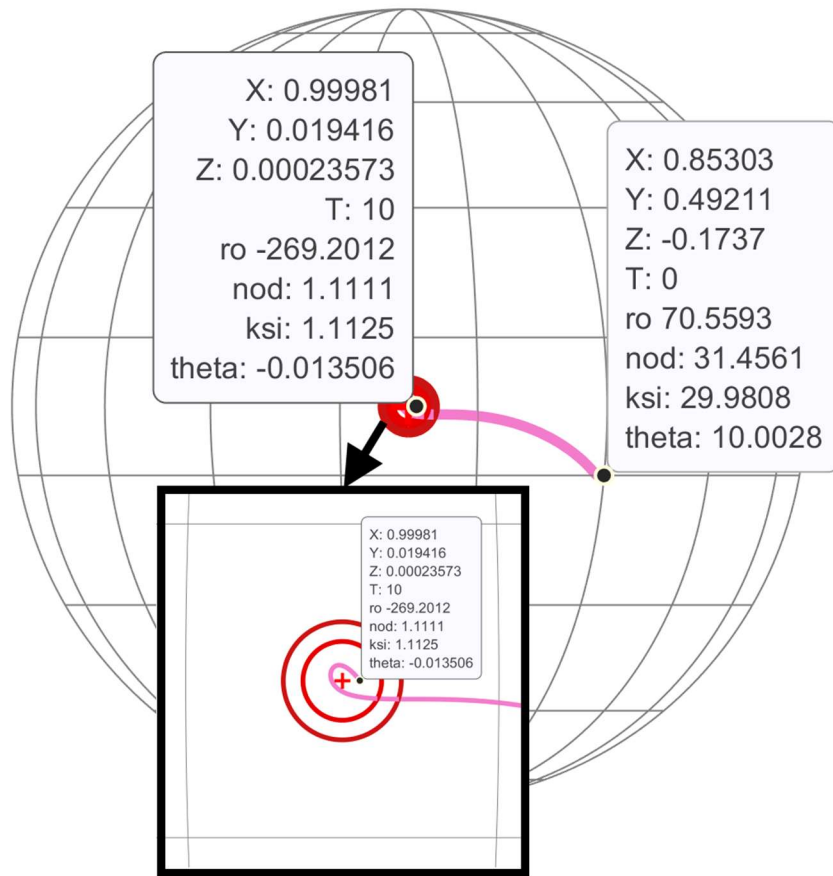


Figure 3.20. Scenario 5 – Path 3D View

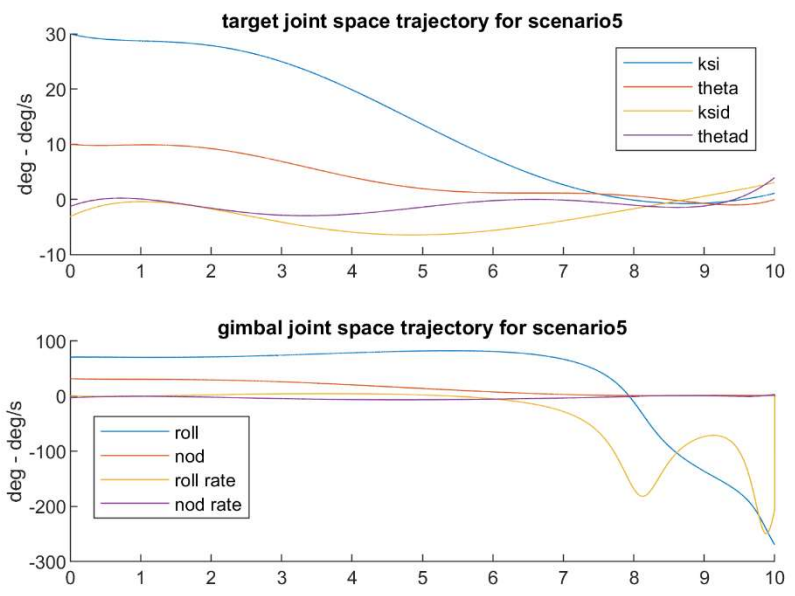


Figure 3.21. Scenario 5 - Trajectories



## CHAPTER 4

### ZENITH PASS ALGORITHMS

Chapter 3 presented simulation topology in detail and provided a basic information on how Zenith Pass Algorithms (ZPA) are placed in it. Referring back to Figure 3.10, there are three ZPAs implemented in the model which are parametrically switched during simulations.

This chapter is devoted to the literature on ZPA and the algorithmic explanation of the proposed solution as a contribution to it.

#### 4.1. Zenith Pass Algorithm Solutions In Literature

Although roll-over-nod gimbals are implemented in many different (commercial and military) applications, there are not too many published works on the solution of ZP problem. The solutions may arise in the form of a patent or a paper investigating a specific type of gimbal, which are far from being general.

It has to be noted that, there are a set of approaches adding a ternary gimbal axis, but those solutions increase the complexity of the system, and therefore not taken into account.

The solutions are based on capturing the onset of nadir cone entrance of the gimbal. When the target (or LOS) enters to the region, a separate algorithm takes the control and generates gimbal commands that are not found by kinematic inversion, but calculated by a different temporal logic.

One common method applied in this temporal logic is locking or limiting roll gimbal movements. This way, only nod gimbal responds to tracker commands and roll becomes unresponsive. The resulting pointing error might be tolerable to some extent, yet it is highly dependent on the target and gimbal dynamics.

In one patent [21] designers choose to add a case discrimination logic which splits the zenith zone into 3 sections. In the innermost section, roll angle is locked. In the middle region, roll rates are limited and in the outer region (rest of the task space) roll rates are not limited. A very similar approach is also utilized in [15]. This work goes one step beyond and verifies effectiveness of the method by experiments. Sensors utilized in the experimental setup are commercial grade. Consequently, the angular rates are limited to 80-100 deg/s, which are quite low values for air-to-air engagement.

It is concluded that the proposed tracking strategy solves the zenith pass problem for a specific case. The study does not present any kind of generalization, parametrization or engagement analysis.

Another way of attacking the problem is presented by P. Savvidis utilizing nonlinear control methods, without a discrimination logic. The singularity is modeled as trigonometric functions in plant model and the controller is expected to overcome this issue. Non-linear generalized minimum variance (NGMV) technique is used to overcome the zenith pass problem. It is explained that the method provides a framework that attempts to isolate the nonlinearities in the system by explicitly including them inside the controller. The NGMV combines features of the Smith Predictor. The uncertainty that might occur between the modeled and the actual plant is regulated with the use of two weightings, penalizing the control and the error signal.

The work shows application details of NGMV on the specific test bench, but neither tries to generalize the problem nor includes the target dynamics, which are the core parts of this dissertation. An important idea obtained from this paper was projecting the target position into a unit sphere located around the gimbal and resolve necessary gimbal angles w.r.t. this sphere. [14]

The most interesting and satisfactory paper found out during literature survey is D. Anderson's work on overcoming zenith pass problem in Directed Infrared Countermeasure (DIRCM) systems. Naturally those type of counter-measures require high performance target tracking, which is parallel to this study. This work aims to use non-conventional control methods to mitigate the effect of zenith singularity on

tracking error. It implements two predictive control algorithms within its control loop. The first is a fast model predictive control in the position loop of the gimbal which minimizes the tracking error by predicting the onset of singularity. The second algorithm predicts the future set-point trajectory, by mostly considering carrier aircraft movements and considering the target as a nearly stable platform. In the final part of the paper, authors compare the performance of the predictive control algorithm with a standard linear approach and underline the effectiveness of the proposed method. [4]

Although the ideas put forward on prediction algorithms for target localization and onset of singularity are fruitful, they are not examined thoroughly. The problem is not parametrized in terms of physical ATTPS properties. However, the use of an unconventional control method (MPC) for generating tracking commands near singularity region is found to be a useful idea. [4]

Another important comment of the study is classification of zenith pass solutions into two groups as path replanning and shooting methods. Path replanning is explained as manipulating the desired sightline trajectory to avoid the zenith zone at the expense of a tracking error, however this type of methods requires a priori knowledge of the trajectory, which is not the case for free target tracking problems. On the other hand, shooting method is explained to be a better strategy by firing the sightline through the zenith by taking preemptive control action. [4]

The above remarkable studies were instrumental in shaping ZPA design.

## **4.2. Baseline Algorithms**

As explained previously, among the three different ZPA's are implemented in the simulation, two of them are used for benchmarking, details of which are explained below:

### 4.2.1. ZPA0

This is the baseline algorithm which includes only kinematic inversion. No special treatment is made for targets getting close to or passing over zenith. Its formulation is given in section 3.1.3.

Although it is an ordinary algorithm, its use is important in verifying whether the existence of others has meaning. Thus, it will be used for basic validation and benchmarking.

Note that both ZPA1 and ZPA2 include ZPA0's kinematic inversion algorithm, but they switch it when required. The flowchart of the algorithm is given below.

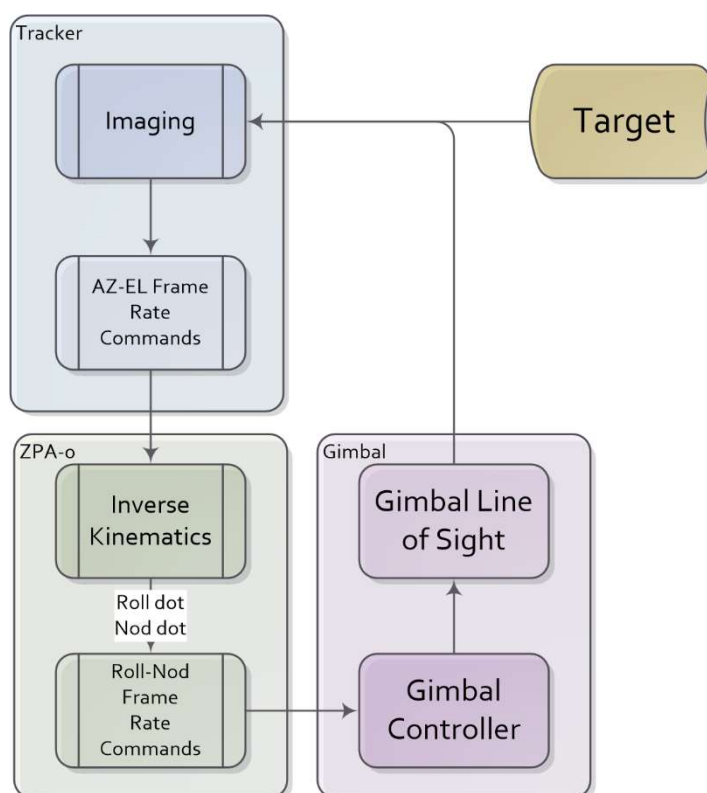


Figure 4.1. ZPA0 Block Diagram

#### **4.2.2. ZPA1**

This algorithm can be regarded as the representation of the standard solutions in literature. Based on a temporal logic controlling nod angle, roll axis movement is locked when the target enters problematic zenith area.

The algorithm constantly monitors gimbal nod angle and when it falls below a certain threshold, it activates ZPA1. Algorithm basically locks roll motions by muting roll rate commands, but continues feeding nod rate commands. With a hysteresis control on nod angle, it deactivates as the nod angle increases.

The algorithm is realized parametrically, in other words the activation zone (nod angle threshold) and maximum allowed gimbal rates can be set programmatically through the simulation. Therefore, regression analysis can be made to observe the effect of ATTPS parameters on ZP performance. Algorithmic block diagram of ZPA1 is given below:

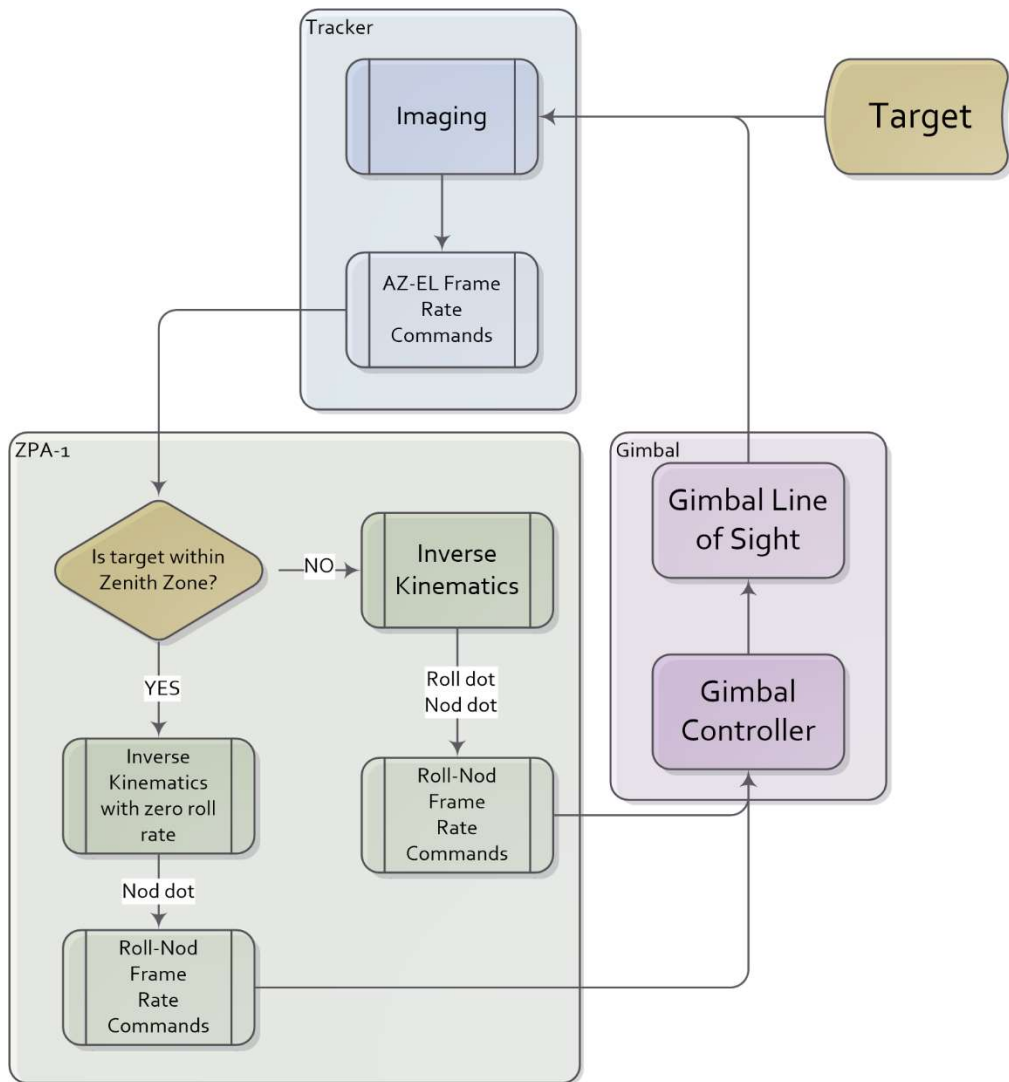


Figure 4.2. ZPA1 Block Diagram

### 4.3. Proposed Zenith Pass Algorithm (ZPA2)

The aim of this study is to achieve a novel algorithm (ZPA2) which outperforms classical methods. After the detailed literature survey, it is decided to design a shooting-based method on which the gimbal is passed from zenith in a controlled fashion. The alternative trajectory will be designed to be non-degenerate. This will ensure that gimbal will pass smoothly through zenith, minimizing LOS error and there will be no wild or uncontrolled motions. [4][22]

ZPA2 includes target state estimator that is invoked at a certain zone, in the form of a Kalman Filter. The workflow is explained by the help of Figure 4.1 below. Here, a near-zenith condition is illustrated.

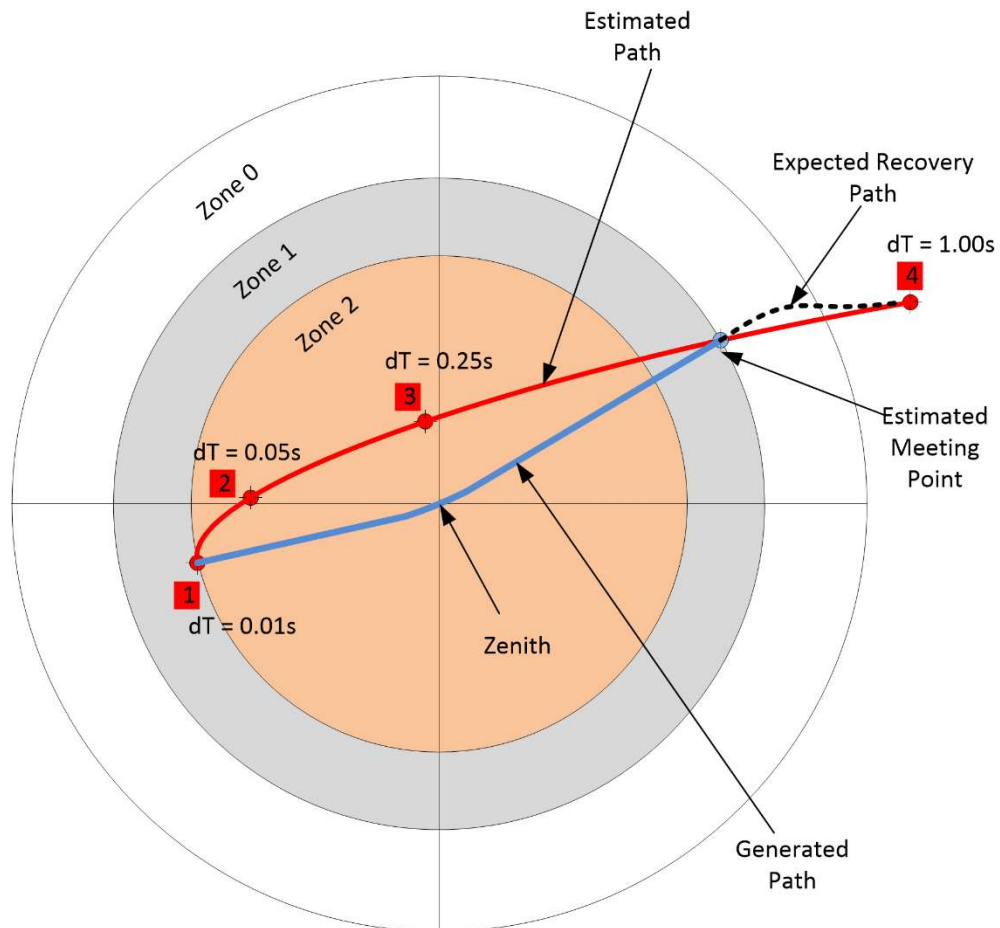


Figure 4.3. ZPA2 Kalman Filter Predictions – Schematic Diagram

Algorithm defines three concentric zones in terms of nod angle. The outer zone (Zone 0) which is significantly away from zenith is used to initiate the Kalman Filter. The filter incorporates a constant acceleration target model. The Kalman filter is corrected at every time step when the system receives a new target information, and that happens with tracker operation frequency, 100 Hz.

The Kalman filter estimates not only angular positions, but also angular rates and accelerations along azimuth and elevation directions. This singularity-free kinematic data will be the aid in generating alternative paths.

When the target enters second zone, Kalman filter starts to generate four different future estimates based on its current state. Those intervals are selected at a geometrically increasing rate as 0.01s, 0.05s, 0.25s and 1s. Those 4 distinct estimates create a trajectory (shown in red) which the target is expected to follow. This makes it possible to foresee the target behavior within nadir cone for a relatively short interval. The estimated values are stored but not actively used until the target enters in the innermost zone (Zone 2)

Zone 2 is used to make the decision to act: (see Figure 4.4)

- If the end of estimated trajectory gets outside the Zone 1 circle;
  - Algorithm takes control from Inverse Kinematics solution,
  - Generates a smooth path which passes from zenith without roll;
  - Follow a smooth path with minimal roll angle and meet with the target at estimated meeting point by satisfying angular rate limits.
- If the estimated trajectory stays inside zenith Zone1 (target stays at near zenith condition)
  - A modified version of IK solution will be used
    - The roll rate command will be multiplied by the absolute value of current nod angle. With small angle assumption, this multiplication will eliminate the sine term in ( 55 ) and damp out wild roll rotations.
  - KF will continue to make estimates
  - If the estimate reaches outside Zone1, switch to the previous state.



The block diagram of ZPA2 is given below

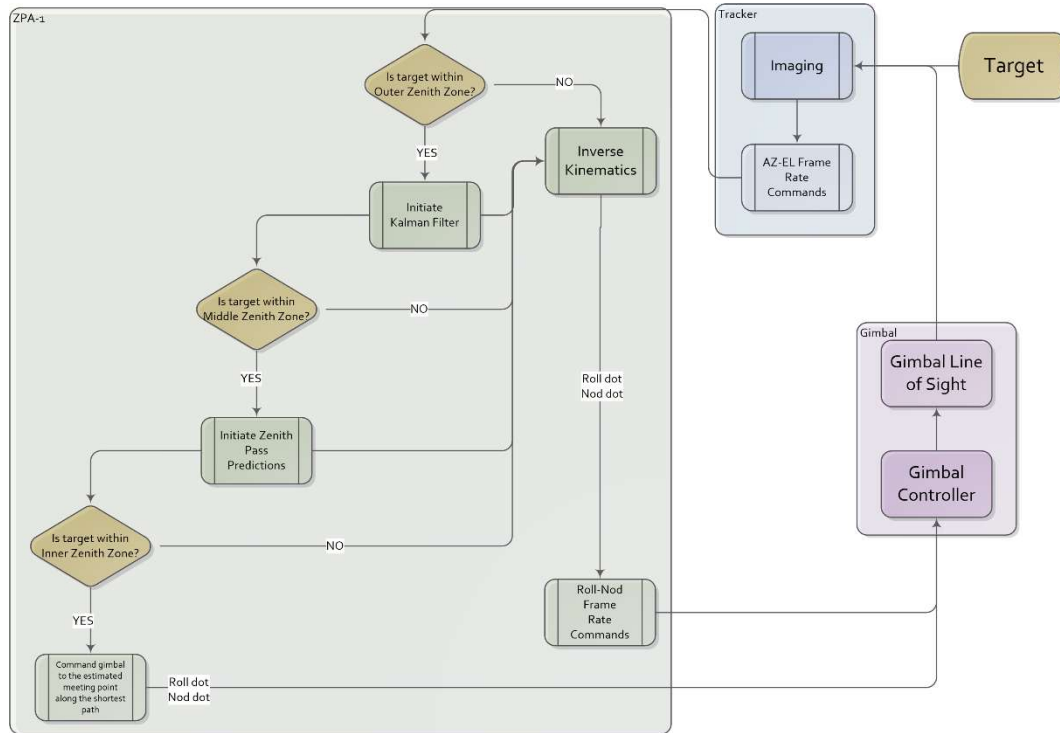


Figure 4.4. ZPA2 Block Diagram

The Kalman Filter formulation is adopted from [23]. As stated earlier, KF operates in singularity-free azimuth-elevation frame which can be approximated as a planar surface in the vicinity of zenith. Therefore, it can be posed as a 2D orthogonal planar state estimation problem. There are 2 linearly independent DOF's as  $\psi$  and  $\theta$ .

Among many motion model alternatives, constant acceleration model is selected, which yields a state vector of size 6:

$$x = \begin{pmatrix} \psi \\ \dot{\psi} \\ \ddot{\psi} \\ \theta \\ \dot{\theta} \\ \ddot{\theta} \end{pmatrix} \quad (64)$$

With the following Kalman Filter definitions, formulation is given as follows:

$\hat{x}_{n+1,n}$ : Predicted system state

$\hat{x}_{n,n}$ : Estimated system state

$z_n$ : Measurement vector

$F$ : State transition matrix

$P_{n+1,n}$ : Predicted covariance matrix

$P_{n,n}$ : Estimated covariance matrix

$Q$ : Process noise matrix

$R$ : Measurement uncertainty matrix

$H$ : Observation matrix

$K_n$ : Kalman gain

For the constant acceleration (CA) model, state transition matrix can be expressed in terms of time interval:

$$F = \begin{bmatrix} 1 & \Delta t & 0.5 \Delta t^2 & 0 & 0 & 0 \\ 0 & 1 & \Delta t & 0 & 0 & 0 \\ 0 & 0 & 1 & 0 & 0 & 0 \\ 0 & 0 & 0 & 1 & \Delta t & 0.5 \Delta t^2 \\ 0 & 0 & 0 & 0 & 1 & \Delta t \\ 0 & 0 & 0 & 0 & 0 & 1 \end{bmatrix} \quad (65)$$

Similarly, if environmental discrete process noise assumed, Q matrix for CA can be derived as follows:

$$Q = \begin{bmatrix} \frac{\Delta t^4}{4} & \frac{\Delta t^3}{3} & \frac{\Delta t^2}{2} & 0 & 0 & 0 \\ \frac{\Delta t^3}{3} & \Delta t^2 & \Delta t & 0 & 0 & 0 \\ \frac{\Delta t^2}{2} & \Delta t & 1 & 0 & 0 & 0 \\ 0 & 0 & 0 & \frac{\Delta t^4}{4} & \frac{\Delta t^3}{3} & \frac{\Delta t^2}{2} \\ 0 & 0 & 0 & \frac{\Delta t^3}{3} & \Delta t^2 & \Delta t \\ 0 & 0 & 0 & \frac{\Delta t^2}{2} & \Delta t & 1 \end{bmatrix} \sigma_a^2 \quad (66)$$

$$H = \begin{bmatrix} 1 & 0 & 0 & 0 & 0 & 0 \\ 0 & 0 & 0 & 1 & 0 & 0 \end{bmatrix} \quad (67)$$

In calculation, following process noise constants are assumed

$$\sigma_a^2 = 3.04 \times 10^{-2} \quad (68)$$

$$R = I_{2 \times 2} \times 0.6 \quad (69)$$

First, the KF is initiated with the following equations. These calculations are done once when the target enters Zone 0

$$\hat{x}_{0,0} = \text{zeros}(6,1) \quad (70)$$

$$P_{0,0} = I_{6 \times 6} \times 1000 \quad (71)$$

Then the recursive predict-correct phase continues as follows:

$$\hat{x}_{n+1,n} = F \hat{x}_{n,n} \quad (72)$$

$$P_{n+1,n} = F P_{n,n} F^T + Q \quad (73)$$

$$z_n = H \hat{x}_{n,n} \quad (74)$$

$$K_n = P_{n,n-1} H^T (H P_{n,n-1} H^T + R_n)^{-1} \quad (75)$$

$$\hat{x}_{n,n} = \hat{x}_{n,n-1} + K_n(z_n - H\hat{x}_{n,n-1}) \quad (76)$$

$$P_{n,n} = (I - K_nH)P_{n,n-1}(I - K_nH)^{-1} + K_nR_nK_n^T \quad (77)$$

When the target gets inside Zone 1, (73) is calculated not for only correction step, but also for several other time steps (0.01, 0.05, 0.25, 1.00) to get target trajectory estimate. In the correction phase only  $\Delta t = 0.01s$  is used.

The formulation is realized in SIMULINK STATEFLOW as depicted in below figure.

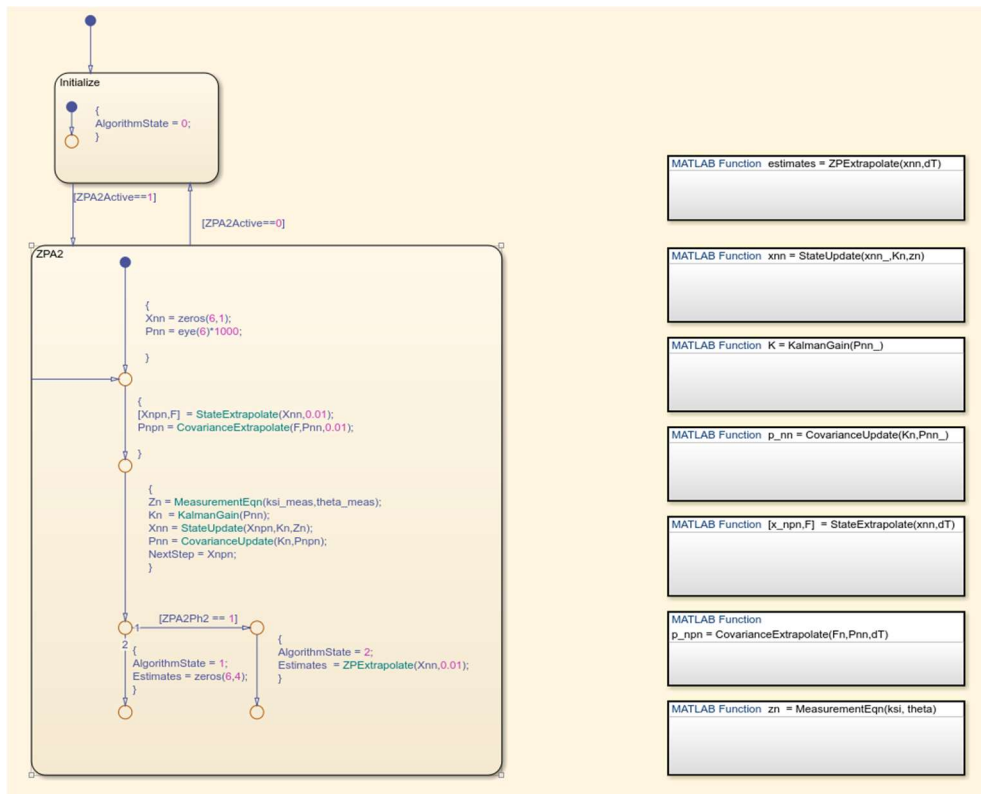


Figure 4.5. ZPA2 implementation in Stateflow

## CHAPTER 5

### TESTS AND VERIFICATION

#### 5.1. Performance criterion

The first and most crucial expectation while performing the tests is keeping the target track on throughout the scenario. As of the beginning, the relevant ZPA algorithm should be able to operate without causing track loss.

The main performance criterion used in the tests is the peak angular rate observed in the rolling axis. This is numerically calculated for each test run.

In some test scenarios, the benchmarking algorithms (ZPA0 or ZPA1) may inherently perform above average. For this reason, when evaluating the results, the algorithm that is compared depending on the scenario can be ZPA0 or ZPA1. The ZPA2 algorithm is expected to perform well in all conditions, regardless of the scenario.

#### 5.2. Test Matrix

The test matrix is constructed with four different variables. These are the scenario, Zenith Pass Algorithm, the gimbal rate limit, and the gimbal rate controller bandwidth, respectively. A series of pre-simulations determined the values used in the relevant test vectors. The test vectors are presented in the table below. As discussed previously, Scenario 4 and 5 are designed as sanity checks for ZPA2

Table 5.1. Test Configurations

Test Vector Element	Scenario	ZPA	RateLimit	Bandwidth
1	Scenario 1	ZPA 0	150 °/s	5 Hz
2	Scenario 2	ZPA 1	300 °/s	10 Hz
3	Scenario 3	ZPA 2	500 °/s	50 Hz
4	Scenario 4 <sup>(*)</sup>		900 °/s	
5	Scenario 5 <sup>(*)</sup>			

(\*): For Scenarios 4 and 5, only ZPA2 is operated.

In order to evaluate the algorithms according to the defined performance criteria, all combinations of the test vectors defined above were tested in the developed simulation environment. In total, 108 different simulations are run.

### 5.3. Test Results

Results of the 108 simulation runs are presented in the below table. The track loss conditions are highlighted in red. Also, peak roll rate column is colored depending on the value. The results are evaluated in the following chapter.

Table 5.2. Test Results

Test	Scenario	ZPA	Rate Limit	Bandwidth	Peak Roll	Track
1	Scn 1	ZPA0	150	5	65,50	1
2	Scn 1	ZPA1	150	5	2,28	1
3	Scn 1	ZPA2	150	5	5,45	1
4	Scn 1	ZPA0	150	10	129,30	1
5	Scn 1	ZPA1	150	10	2,79	1
6	Scn 1	ZPA2	150	10	20,48	1
7	Scn 1	ZPA0	150	50	181,98	0
8	Scn 1	ZPA1	150	50	4,00	1
9	Scn 1	ZPA2	150	50	17,05	1
10	Scn 1	ZPA0	300	5	20,07	1
11	Scn 1	ZPA1	300	5	2,89	1
12	Scn 1	ZPA2	300	5	5,87	1
13	Scn 1	ZPA0	300	10	89,11	1
14	Scn 1	ZPA1	300	10	3,82	1

Test	Scenario	ZPA	Rate Limit	Bandwidth	Peak Roll	Track
15	Scn 1	ZPA2	300	10	38,45	1
16	Scn 1	ZPA0	300	50	359,80	0
17	Scn 1	ZPA1	300	50	4,37	1
18	Scn 1	ZPA2	300	50	22,15	1
19	Scn 1	ZPA0	500	5	115,30	1
20	Scn 1	ZPA1	500	5	2,70	1
21	Scn 1	ZPA2	500	5	17,54	1
22	Scn 1	ZPA0	500	10	258,37	1
23	Scn 1	ZPA1	500	10	2,83	1
24	Scn 1	ZPA2	500	10	26,99	1
25	Scn 1	ZPA0	500	50	581,62	0
26	Scn 1	ZPA1	500	50	3,19	1
27	Scn 1	ZPA2	500	50	29,62	1
28	Scn 1	ZPA0	900	5	201,48	1
29	Scn 1	ZPA1	900	5	2,05	1
30	Scn 1	ZPA2	900	5	10,15	1
31	Scn 1	ZPA0	900	10	429,80	1
32	Scn 1	ZPA1	900	10	2,50	1
33	Scn 1	ZPA2	900	10	12,03	1
34	Scn 1	ZPA0	900	50	1018,44	0
35	Scn 1	ZPA1	900	50	3,27	1
36	Scn 1	ZPA2	900	50	16,17	1
37	Scn 2	ZPA0	150	5	179,51	0
38	Scn 2	ZPA1	150	5	122,40	1
39	Scn 2	ZPA2	150	5	83,38	1
40	Scn 2	ZPA0	150	10	180,05	0
41	Scn 2	ZPA1	150	10	131,57	1
42	Scn 2	ZPA2	150	10	109,91	1
43	Scn 2	ZPA0	150	50	183,51	0
44	Scn 2	ZPA1	150	50	163,28	0
45	Scn 2	ZPA2	150	50	108,14	1
46	Scn 2	ZPA0	300	5	318,18	0
47	Scn 2	ZPA1	300	5	121,92	1
48	Scn 2	ZPA2	300	5	88,91	1
49	Scn 2	ZPA0	300	10	314,67	0
50	Scn 2	ZPA1	300	10	150,65	1
51	Scn 2	ZPA2	300	10	83,52	1
52	Scn 2	ZPA0	300	50	306,10	0
53	Scn 2	ZPA1	300	50	159,10	1
54	Scn 2	ZPA2	300	50	100,69	1
55	Scn 2	ZPA0	500	5	532,49	0

Test	Scenario	ZPA	Rate Limit	Bandwidth	Peak Roll	Track
56	Scn 2	ZPA1	500	5	139,01	1
57	Scn 2	ZPA2	500	5	81,73	1
58	Scn 2	ZPA0	500	10	527,24	0
59	Scn 2	ZPA1	500	10	147,30	1
60	Scn 2	ZPA2	500	10	90,17	1
61	Scn 2	ZPA0	500	50	512,28	0
62	Scn 2	ZPA1	500	50	158,45	1
63	Scn 2	ZPA2	500	50	85,93	1
64	Scn 2	ZPA0	900	5	951,74	0
65	Scn 2	ZPA1	900	5	138,15	1
66	Scn 2	ZPA2	900	5	82,96	1
67	Scn 2	ZPA0	900	10	920,19	0
68	Scn 2	ZPA1	900	10	148,42	1
69	Scn 2	ZPA2	900	10	95,29	1
70	Scn 2	ZPA0	900	50	759,71	1
71	Scn 2	ZPA1	900	50	162,27	1
72	Scn 2	ZPA2	900	50	113,54	1
73	Scn 3	ZPA0	150	5	156,41	0
74	Scn 3	ZPA1	150	5	164,71	0
75	Scn 3	ZPA2	150	5	157,68	0
76	Scn 3	ZPA0	150	10	154,72	0
77	Scn 3	ZPA1	150	10	165,02	0
78	Scn 3	ZPA2	150	10	152,34	0
79	Scn 3	ZPA0	150	50	152,41	0
80	Scn 3	ZPA1	150	50	166,76	0
81	Scn 3	ZPA2	150	50	173,44	0
82	Scn 3	ZPA0	300	5	314,02	0
83	Scn 3	ZPA1	300	5	292,62	0
84	Scn 3	ZPA2	300	5	180,20	1
85	Scn 3	ZPA0	300	10	309,61	0
86	Scn 3	ZPA1	300	10	315,90	0
87	Scn 3	ZPA2	300	10	191,24	1
88	Scn 3	ZPA0	300	50	303,32	0
89	Scn 3	ZPA1	300	50	333,51	0
90	Scn 3	ZPA2	300	50	183,72	1
91	Scn 3	ZPA0	500	5	414,61	1
92	Scn 3	ZPA1	500	5	165,46	0
93	Scn 3	ZPA2	500	5	195,34	1
94	Scn 3	ZPA0	500	10	375,03	1
95	Scn 3	ZPA1	500	10	314,69	0
96	Scn 3	ZPA2	500	10	171,42	1



Test	Scenario	ZPA	Rate Limit	Bandwidth	Peak Roll	Track
97	Scn 3	ZPA0	500	50	350,59	1
98	Scn 3	ZPA1	500	50	336,09	0
99	Scn 3	ZPA2	500	50	186,10	1
100	Scn 3	ZPA0	900	5	413,62	1
101	Scn 3	ZPA1	900	5	290,93	0
102	Scn 3	ZPA2	900	5	184,05	1
103	Scn 3	ZPA0	900	10	370,86	1
104	Scn 3	ZPA1	900	10	316,43	0
105	Scn 3	ZPA2	900	10	175,17	1
106	Scn 3	ZPA0	900	50	357,92	1
107	Scn 3	ZPA1	900	50	340,98	0
108	Scn 3	ZPA2	900	50	182,31	1



## CHAPTER 6

### RESULTS AND DISCUSSION

#### 6.1. Performance of Zenith Pass Algorithms

When the results were examined, the ZPA2 was successful in all test conditions except three without losing target tracking. However, depending on the scenario, the test conditions for which ZPA0 and ZPA1 lost track were numerous. The maximum roll rate is the key performance metric to quantify the results. From this point of view, the ZPA2 showed high performance.

Since each scenario provides a different perspective, the results are evaluated scenario-based.

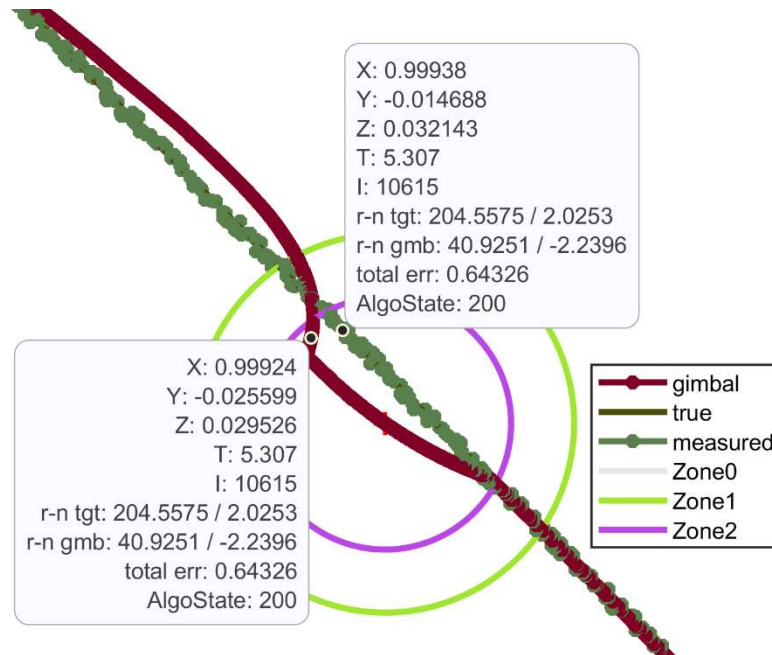


Figure 6.1. Results of an exemplary scenario run -Trajectory (ZPA2, Scenario 2)

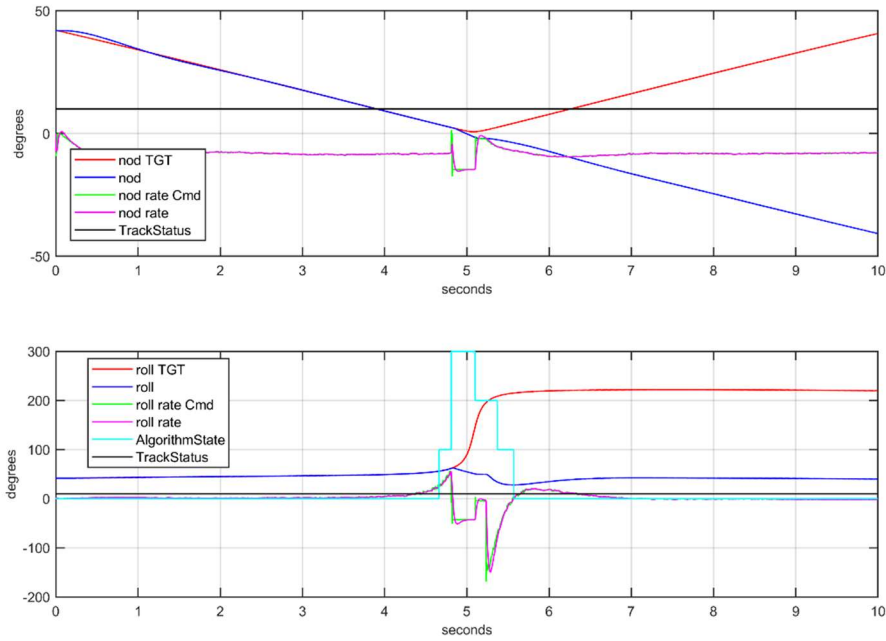


Figure 6.2. Results of an exemplary scenario run -Test Data (ZPA2, Scenario 2)

The results of a single test run can be graphically visualized as in the above figures. For presenting a total of 108 tests, key performance metrics are calculated and the results are tabulated.

As expected, the ZPA0 algorithm performed poorly in the Scenario 1 tests representing the exact zenith-pass condition. Infinitesimal errors due to measurement noise caused huge roll commands and hindered tracking. On the other hand, ZPA1 and ZPA2 algorithms successfully tracked the target by deriving very low roll rate commands.

Table 6.1. Scenario 1 results (ZPA0 vs ZPA2)

Test	Scenario	ZPA	Rate Limit	Bandwidth	Peak Roll	Track
1	Scn 1	ZPA0	150	5	65,50	1
3	Scn 1	ZPA2	150	5	5,45	1
4	Scn 1	ZPA0	150	10	129,30	1
6	Scn 1	ZPA2	150	10	20,48	1
7	Scn 1	ZPA0	150	50	181,98	0

9	Scn 1	ZPA2	150	50	17,05	1
10	Scn 1	ZPA0	300	5	20,07	1
12	Scn 1	ZPA2	300	5	5,87	1
13	Scn 1	ZPA0	300	10	89,11	1
15	Scn 1	ZPA2	300	10	38,45	1
16	Scn 1	ZPA0	300	50	359,80	0
18	Scn 1	ZPA2	300	50	22,15	1
19	Scn 1	ZPA0	500	5	115,30	1
21	Scn 1	ZPA2	500	5	17,54	1
22	Scn 1	ZPA0	500	10	258,37	1
24	Scn 1	ZPA2	500	10	26,99	1
25	Scn 1	ZPA0	500	50	581,62	0
27	Scn 1	ZPA2	500	50	29,62	1
28	Scn 1	ZPA0	900	5	201,48	1
30	Scn 1	ZPA2	900	5	10,15	1
31	Scn 1	ZPA0	900	10	429,80	1
33	Scn 1	ZPA2	900	10	12,03	1
34	Scn 1	ZPA0	900	50	1018,44	0
36	Scn 1	ZPA2	900	50	16,17	1

Especially in Scenario 2 tests simulating the close-zenith-pass situation, the designed ZPA2 algorithm derived much lower roll rate commands than ZPA0. The difference is on the order of 3 to 10 times. The difference in rate command clearly indicates how the use of a suitable zenith pass algorithm affects target tracking performance and gimbal control.

Table 6.2. Scenario 2 results (ZPA0 vs ZPA2)

Test	Scenario	ZPA	Rate		Peak Roll	Track
			Limit	Bandwidth		
37	Scn 2	ZPA0	150	5	179,51	0
39	Scn 2	ZPA2	150	5	83,38	1
40	Scn 2	ZPA0	150	10	180,05	0
42	Scn 2	ZPA2	150	10	109,91	1
43	Scn 2	ZPA0	150	50	183,51	0
45	Scn 2	ZPA2	150	50	108,14	1
46	Scn 2	ZPA0	300	5	318,18	0
48	Scn 2	ZPA2	300	5	88,91	1
49	Scn 2	ZPA0	300	10	314,67	0
51	Scn 2	ZPA2	300	10	83,52	1
52	Scn 2	ZPA0	300	50	306,10	0

54	Scn 2	ZPA2	300	50	100,69	1
55	Scn 2	ZPA0	500	5	532,49	0
57	Scn 2	ZPA2	500	5	81,73	1
58	Scn 2	ZPA0	500	10	527,24	0
60	Scn 2	ZPA2	500	10	90,17	1
61	Scn 2	ZPA0	500	50	512,28	0
63	Scn 2	ZPA2	500	50	85,93	1
64	Scn 2	ZPA0	900	5	951,74	0
66	Scn 2	ZPA2	900	5	82,96	1
67	Scn 2	ZPA0	900	10	920,19	0
69	Scn 2	ZPA2	900	10	95,29	1
70	Scn 2	ZPA0	900	50	759,71	1
72	Scn 2	ZPA2	900	50	113,54	1

For Scenario 3, which simulates the far-zenith-pass situation, comparing ZPA1 and ZPA2 is meaningful. The ZPA1 algorithm failed in almost all of these tests. When the roll axis was locked after algorithm was triggered, tracking was lost as the gimbal was cued to the zenith circle's opposite side. On the other hand, since the ZPA2 algorithm could predict the exit point of the zenith zone, it moved the gimbal by targeting this point and kept track. Test cases where the ZPA2 algorithm fails are the ones with the lowest speed limit, 150 degrees/second. Other than that, there has yet to be a test case where ZPA2 failed.

Table 6.3. Scenario 3 results (ZPA1 vs ZPA2)

Test	Scenario	ZPA	Rate Limit	Bandwidth	Peak Roll	Track
74	Scn 3	ZPA1	150	5	164,71	0
75	Scn 3	ZPA2	150	5	157,68	0
77	Scn 3	ZPA1	150	10	165,02	0
78	Scn 3	ZPA2	150	10	152,34	0
80	Scn 3	ZPA1	150	50	166,76	0
81	Scn 3	ZPA2	150	50	173,44	0
83	Scn 3	ZPA1	300	5	292,62	0
84	Scn 3	ZPA2	300	5	180,20	1
86	Scn 3	ZPA1	300	10	315,90	0
87	Scn 3	ZPA2	300	10	191,24	1
89	Scn 3	ZPA1	300	50	333,51	0
90	Scn 3	ZPA2	300	50	183,72	1

92	Scn 3	ZPA1	500	5	165,46	0
93	Scn 3	ZPA2	500	5	195,34	1
95	Scn 3	ZPA1	500	10	314,69	0
96	Scn 3	ZPA2	500	10	171,42	1
98	Scn 3	ZPA1	500	50	336,09	0
99	Scn 3	ZPA2	500	50	186,10	1
101	Scn 3	ZPA1	900	5	290,93	0
102	Scn 3	ZPA2	900	5	184,05	1
104	Scn 3	ZPA1	900	10	316,43	0
105	Scn 3	ZPA2	900	10	175,17	1
107	Scn 3	ZPA1	900	50	340,98	0
108	Scn 3	ZPA2	900	50	182,31	1

Finally, the resistance of the ZPA2 algorithm to challenging target movements was tested with Scenario 4 and Scenario 5 analysis.

In the analysis of Scenario 4, the trajectory given below, the behavior of the ZPA2 algorithm is seen. Although the algorithm entered the zenith circle, it detected that the target did not move toward the center and continued to use the IK solution.

Here, ZPA2 is operated at 500 deg/s rate limit and 10Hz rate bandwidth. As it is clearly seen in Figure 6.1 and Figure 6.2, ZPA2 is invoked inside the zenith circle (AlgoState being 200 means the algorithm started, Kalman Filter giving estimates on the exit location), however it is robust for this tangential pass.

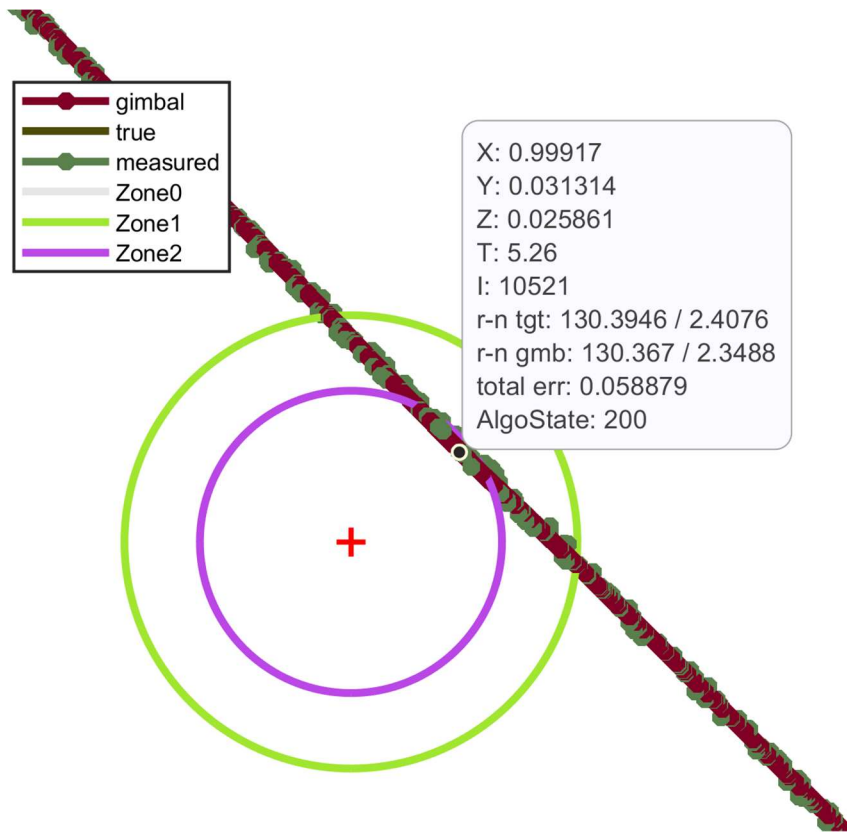


Figure 6.3. ZPA2 performance under Scenario 4. Trajectory

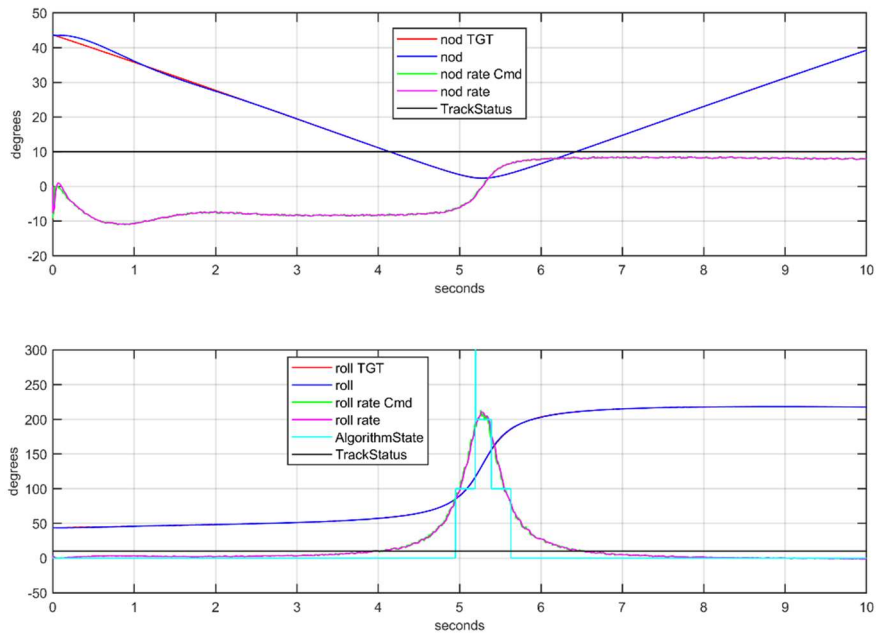


Figure 6.4. ZPA2 performance under Scenario 4. Test Data



Similarly, in the images containing the Scenario 5 analysis, it can be seen that the target entering the zenith circle and remaining there does not cause an unexpected jump in the algorithm, and the gimbal stability is ensured.

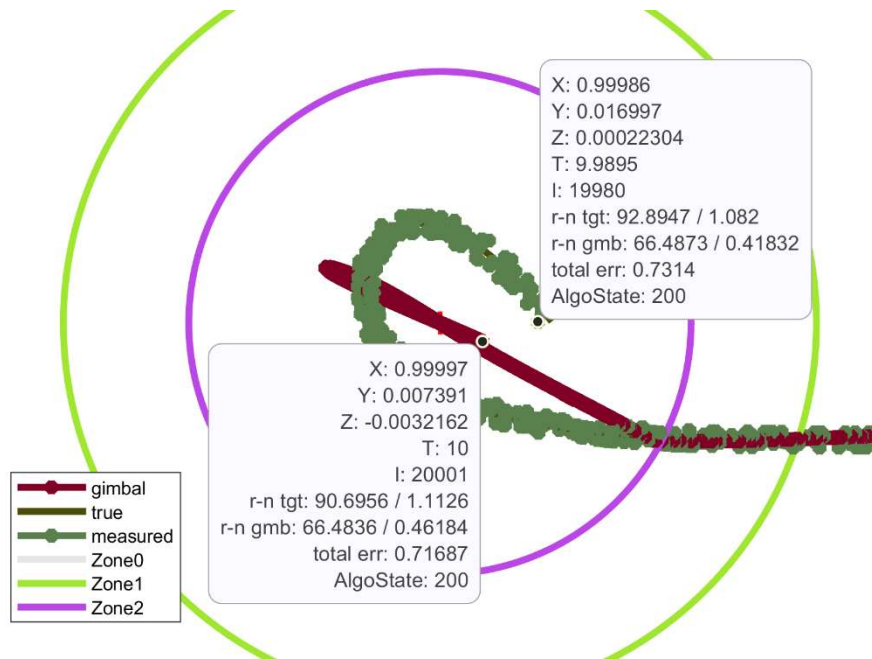


Figure 6.5. ZPA2 performance under Scenario 5. Trajectory

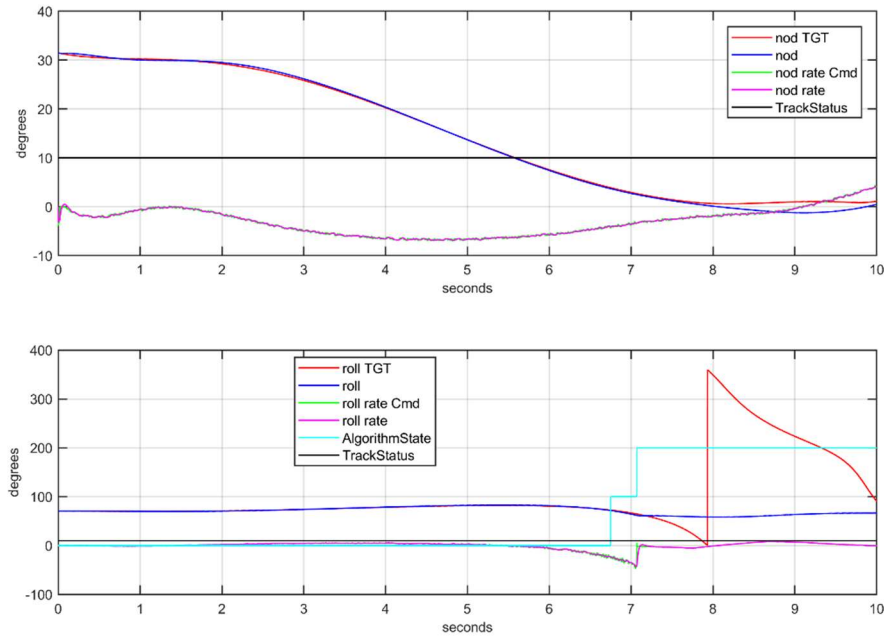


Figure 6.6. ZPA2 performance under Scenario 5. Test data

## 6.2. Discussion

In this thesis study;

- The zenith pass problem in roll-nod configuration gimbals has been investigated.
- System variables on which the problem is dependent were examined.
- Work was carried out with a focus on air-to-air engagement, as this problem is known to be pronounced, especially in long focal length, narrow-angle air-to-air missile gimbals.
- Engagement condition has been mathematically simplified and mapped onto a unit sphere, and a comprehensive simulation environment including all critical variables has been created to perform the studies. In this environment, a realistic target-missile match is simulated, and the behavior of the gimbal controller and zenith pass algorithm can be observed.

- A novel zenith pass algorithm has been designed, including a Kalman Filter with a constant acceleration model. Two baseline algorithms in the literature were found for comparison.
- A multivariate test matrix was created with critical system parameters, and the algorithms were tested respectively in the developed simulation environment.
- The results were evaluated, showing that the proposed method was successful.

### **6.3. Further Study**

As mentioned in the previous chapters, the most important outputs of this study are the simulation environment produced and the ZPA2 algorithm. The scenarios used were chosen as compelling to simulate the air-air engagement. As a continuation of this work, the algorithm's performance can be observed in more realistic conditions by feeding a real air-to-air engagement scenario to the developed simulation environment. The derivation or obtaining of the mentioned engagement data was not possible within the scope of the thesis study.

As described in Chapter 4 on the ZPA2 algorithm design, the algorithm that predicts target movements uses the constant acceleration model. Today, the Interacting Multiple Model (IMM) model is widely used for target state estimation. Its performance can be improved by updating the target model in the proposed algorithm with IMM.

Another development effort could be to derive more compelling synthetic scenarios for improving the logic flow and stability of the algorithm. This work, which needs to strike a balance between realism and compelling, is critical for Zenith Pass Algorithm designs. For the mentioned purpose, Scenario 4 and Scenario 5 are derived in this thesis study. By continuing this work, the control logic of the algorithm can be improved with more challenging target movements.

Finally, the zenith pass problem can be studied on different types of gimbals by changing the isolated air-to-air missile gimbal model in the developed simulation environment. For example, the gimbal given in Figure 1.1 is a pedestal turret designed to track air targets from the ground and has an elevation angle limit. Although this system cannot mechanically pass through the zenith, it may lose track by getting stuck at the speed limit near the zenith while the targets pass over it. Using the simulation environment developed in this thesis, other algorithms can be designed for limited-angle turrets to track targets passing through the zenith point.

## REFERENCES

- [1] Hurák Z, Řezáč M. Image-based pointing and tracking for inertially stabilized airborne camera platform. *IEEE Trans Control Syst Technol* 2012;20:1146–59. <https://doi.org/10.1109/TCST.2011.2164541>.
- [2] Siouris GM. Missile Guidance and Control Systems. *Appl Mech Rev* 2004;57:B32. <https://doi.org/10.1115/1.1849174>.
- [3] Moody L. Sensors, measurement fusion and missile trajectory optimisation. 2003. <https://doi.org/10.1260/0957456042880200>.
- [4] Anderson D, McGookin M, Brignall N. Fast Model Predictive Control of the Nadir Singularity in Electro-Optic Systems. *J Guid Control Dyn* 2009;32:626–32. <https://doi.org/10.2514/1.30762>.
- [5] Bigley WJ, Schupan F. Wideband Base Motion Isolation Control for a Mobile Platform. *Proc Am Control Conf* 1987:1483–90.
- [6] Kun Z, Hexi B. Study of zenith pass problem of the inter-satellite linkage antenna. 2008 10th Int Conf Control Autom Robot Vision, ICARCV 2008 2008;317:317–22. <https://doi.org/10.1109/ICARCV.2008.4795539>.
- [7] Crawford PS, Brush RJH. Trajectory optimisation to minimise antenna pointing error. *Comput Control Eng J* 1995;6:61–7. <https://doi.org/10.1049/cce:19950201>.
- [8] Zlatanov DS. Generalized Singularity Analysis of Mechanisms. University of Toronto, 1998.
- [9] Reiter A. Optimal Path and Trajectory Planning for Serial Robots. Wiesbaden: Springer Fachmedien Wiesbaden; 2020. <https://doi.org/10.1007/978-3-658-28594-4>.
- [10] Oetomo D, Ang Jr MH. Singularity robust algorithm in serial manipulators. *Robot Comput Integr Manuf* 2009;25:122–34. <https://doi.org/10.1016/j.rcim.2007.09.007>.

- [11] Nadal OB. Numerical Computation and Avoidance of Manipulator Singularities. Universidad Politécnica de Cataluña, 2013.
- [12] Kandemir KD, Yazicioglu Y, Özkan B. Kinematic analysis of imaging seekers with roll-over-nod gimbal and a folded electro-optical layout. In: Hickman DL, Bürsing H, editors. Electro-Optical Infrared Syst. Technol. Appl. XVI, SPIE; 2019, p. 26. <https://doi.org/10.1117/12.2532791>.
- [13] Siciliano B, Sciavicco L, Villani L, Oriolo G. Robotics; Modelling, Planning and Control. London: Springer London; 2009. <https://doi.org/10.1007/978-1-84628-642-1>.
- [14] Savvidis P, Anderson D, Grimble M. Application of nonlinear generalised minimum variance to the nadir problem in 2-axis gimbal pointing and stabilization. SPIE Defense, ... 2010;7696:76961I. <https://doi.org/10.1117/12.849523>.
- [15] Jiang H, Jia H, Wei Q. Analysis of zenith pass problem and tracking strategy design for roll-pitch seeker. Aerosp Sci Technol 2012;23:345–51. <https://doi.org/10.1016/j.ast.2011.08.011>.
- [16] Imado F, Uehara S. High-g barrel roll maneuvers against proportional navigation from optimal control viewpoint. J Guid Control Dyn 1998;21:876–81. <https://doi.org/10.2514/2.4351>.
- [17] Yoon S, Lundberg J, Ekstrand B. Equations of motion for a two-axes gimbal system. IEEE Trans Aerosp Electron Syst 2001;37:1083–1091. <https://doi.org/10.1109/7.953259>.
- [18] Skoglar P. Modelling and control of IR / EO-gimbal for UAV surveillance applications. Linköping Institute of Technology, Linköping, Sweden, 2002.
- [19] Hilkert JM. Precision Stabilized Pointing and Tracking Systems. 2017.
- [20] Masten MK. Inertially Stabilized Platforms for Optical Imaging Systems Tracking Dynamic Targets with Mobile Sensors. IEEE Control Syst 2008;28:47–64. <https://doi.org/10.1109/MCS.2007.910201>.

- [21] Hartmann U, Schnatz J, Goseberg H. Seeker for target-tracking missiles. US6978965B1, 2005.
- [22] Nenchev DN, Tsumaki Y, Uchiyama M. Singularity-Consistent Parameterization of Robot Motion and Control. *Int J Rob Res* 2000;19:159–82. <https://doi.org/10.1177/02783640022066806>.
- [23] Becker A. KalmanFilter.NET 2022. <https://www.kalmanfilter.net/multiExamples.html>.





## CURRICULUM VITAE

Surname, Name: Kandemir, Kutlu Demir

### EDUCATION

Degree	Institution	Year of Graduation
MS	METU Mechanical Engineering	2010
BS	METU Mechanical Engineering	2007
High School	Ankara Atatürk High School, Ankara	2003

### FOREIGN LANGUAGES

Advanced English,

### PUBLICATIONS

1. Kandemir, Kutlu Demir, Alper Akmese, and Yigit Yazicioglu. "Line-of-sight stabilization of a gimbaled mechanism under passive base isolation." *Proceedings of the Institution of Mechanical Engineers, Part G: Journal of Aerospace Engineering* 228.1 (2014): 35-43.
2. Kandemir, Kutlu D., Yigit Yazicioglu, and Bulent Ozkan. "Kinematic analysis of imaging seekers with roll-over-nod gimbal and a folded electro-optical layout." *Electro-Optical and Infrared Systems: Technology and Applications XVI*. Vol. 11159. SPIE, 2019.